

A synthetic methylotroph achieves accelerated cell growth by alleviating transcription-replication conflicts

Received: 11 May 2024

Accepted: 13 December 2024

Published online: 02 January 2025

 Check for updatesXin Meng¹, Guipeng Hu², Xiaomin Li¹, Cong Gao¹, Wei Song²,
Wanqing Wei¹, Jing Wu² & Liming Liu¹✉

Microbial utilization of methanol for valorization is an effective way to advance green bio-manufacturing technology. Although synthetic methylotrophs have been developed, strategies to enhance their cell growth rate and internal regulatory mechanism remain underexplored. In this study, we design a synthetic methanol assimilation (SMA) pathway containing only six enzymes linked to central carbon metabolism, which does not require energy and carbon emissions. Through rational design and laboratory evolution, *E. coli* harboring with the SMA pathway is converted into a synthetic methylotroph. By self-adjusting the expression of TOPAI (topoisomerase I inhibitor) to alleviate transcriptional-replication conflicts (TRCs), the doubling time of methylotrophic *E. coli* is reduced to 4.5 h, approaching that of natural methylotrophs. This work has the potential to overcome the growth limitation of C1-assimilating microbes and advance the development of a circular carbon economy.

The development of green bio-manufacturing technology is one of the important ways to address energy and environmental challenges. Currently, bio-manufacturing primarily uses saccharic raw materials, which compete with human food resources. To address this issue, one-carbon (C1) compounds derived from CO₂ and other renewable sources are selected as alternative feedstocks for chemical production^{1,2}. The utilization of C1 compounds, such as methanol, for microbial growth and chemical production is expected to significantly advance carbon neutrality and the circular carbon economy.

C1 biotransformation offers an ideal approach for the valorization of C1 compounds in the synthesis of biomass, biofuels and chemicals³. Natural methylotrophs, such as *Bacillus methanolicus*, can utilize methanol for cell growth and metabolism, but they present challenges for genetic modification into versatile cell factories for diverse chemicals production^{4,5}. In contrast, biotechnological work-horses like *Escherichia coli* and *Saccharomyces cerevisiae*, possess higher plasticity and a wide range of genetic modification tools, making them promising candidates for C1 utilization and biomanufacturing^{6,7}. Recent research has focused on developing these model microorganisms into

platform for C1 assimilation by introducing homologous or heterologous natural assimilation pathways to enable cell growth and chemical production^{8–29}. Among these, the ribulose monophosphate (RuMP) cycle is recognized as the most efficient methanol assimilation pathway^{8,21,30}, however, the carbon yield of acetyl-CoA derivatives is limited due to CO₂ emissions. To address these issues, strategies combining of computer-aided design and protein engineering have been explored to create artificial assimilation pathways for the efficient utilization of C1 feedstocks^{31–34}. While many of these artificial pathways have been validated in vitro, they often lack assimilation capacity in vivo, such as *E. coli*³⁵. Recently, artificial assimilation pathways have been designed not only to overcome compensate for existing limitations, but also to create synthetic methylotrophs or C1-assimilating cell factories through metabolic engineering and adaptive evolution. Despite these advances, synthetic methylotrophs still face challenges such as metabolite toxicity and insufficient cell growth^{13,25–27}. However, only a few mechanisms have been elucidated that enhance cell growth, such as the alleviation of DNA-protein crosslinking (DPC), and modifications to cell membrane components^{23–27}. Therefore, it is essential

¹School of Biotechnology and Key Laboratory of Industrial Biotechnology of Ministry of Education, Jiangnan University, Wuxi, China. ²School of Life Sciences and Health Engineering, Jiangnan University, Wuxi, China. ✉e-mail: mingll@jiangnan.edu.cn

to conduct a deeper analysis of the underlying molecular mechanisms in artificial methylotrophs and to develop strategies that can improve cell growth on methanol.

In this work, a six-enzyme SMA pathway is designed and constructed to synthesize acetyl-CoA from methanol without carbon emissions. Following the introduction of this pathway into *E. coli*, a combination of rational design and genome-targeting mutator strategy (GTMS) with adaptive laboratory evolution (ALE) is used to develop synthetic methylotrophs. Omics sequencing reveals that the alleviation of transcriptional-replication conflicts (TRCs) shortens the doubling time of methylotrophic *E. coli* to 4.5 h. These findings provide valuable insights into the molecular mechanism by which synthetic methylotrophs achieve accelerated cell growth.

Results

Design and construction of the SMA pathway

In order to increase the utilize of methanol by *E. coli*, a synthetic methanol assimilation (SMA) pathway was designed through a rational combination of methanol assimilation and carbon-neutral metabolism.

As illustrated in Fig. 1a, the SMA pathway consisted of three metabolic modules containing six enzymes that catalyzed methanol (C1) to acetyl-CoA (C2): (1) Methanol oxidation module (Module I), which was constructed by methanol dehydrogenase (MDH)³⁶, oxidize methanol to formaldehyde (C1); (2) Formaldehyde fixation module (Module II), which combined glycolaldehyde synthase (GALS)³⁴, hexose-6-phosphate aldolase (HSA) and hexose phosphate isomerase (PHI), catalyze two molecules of formaldehyde with one molecule of erythrose 4-phosphate (E4P) (C4) to synthesize one molecule of fructose-6-phosphate (F6P) (C6), achieving the conversion of 2C1 + C4 to C6; (3) Carbon rearrangement module (Module III), consisting of fructose-5-phosphate phosphoketolase (FPK)³¹ and phosphotransacetylase (PTA), converted F6P into E4P and acetyl-CoA (C2), achieving the conversion of C6 to C4 + C2. E4P is regenerated and re-enters enter the next cycle, while acetyl-CoA serves as an output and is a precursor to biomass synthesis.

The feasibility of the SMA pathway was verified from five key aspects. First, the total Gibbs free energy of the whole reaction was approximately $-78.2 \text{ kJ mol}^{-1}$, indicating that the SMA pathway was

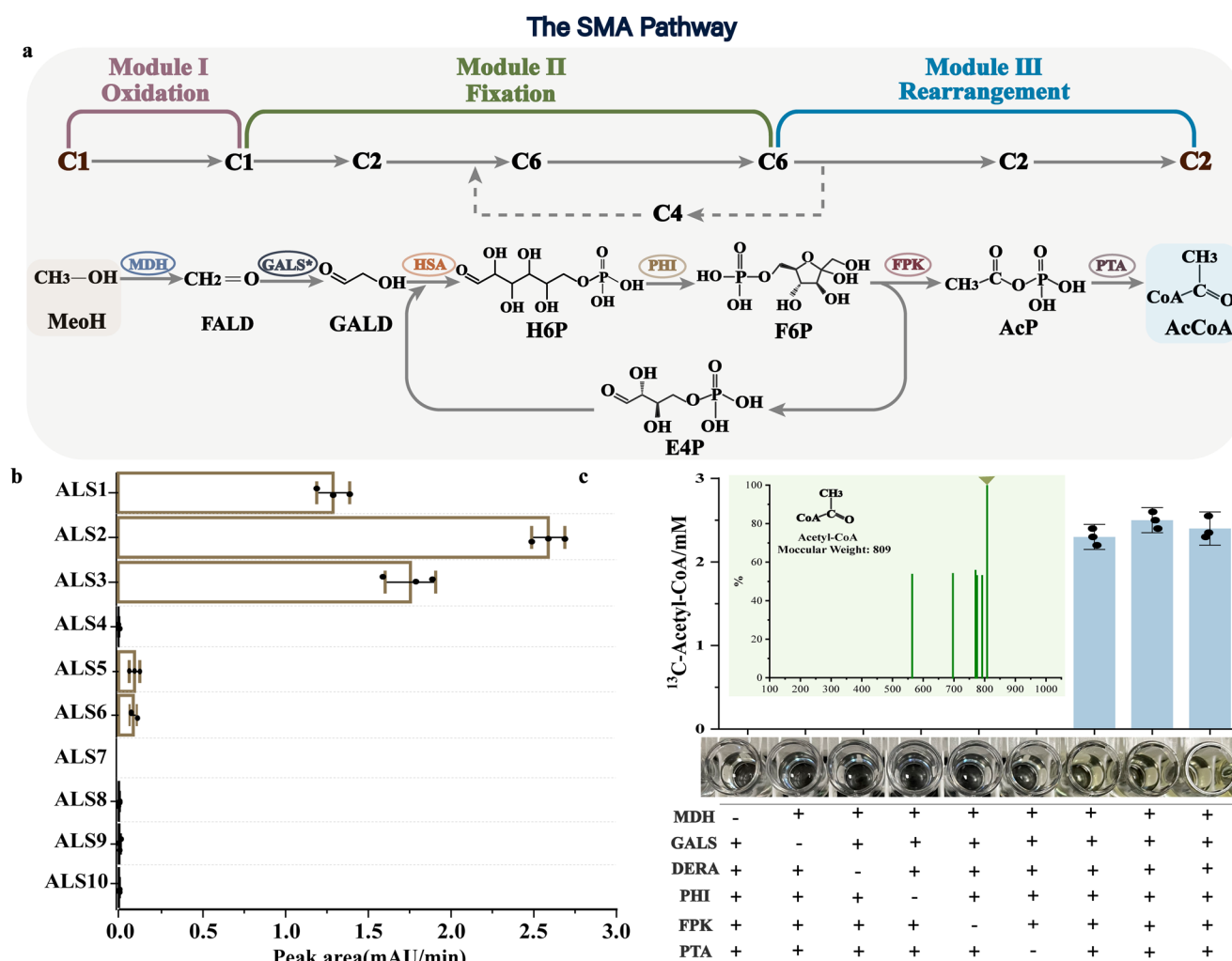


Fig. 1 | Design and construction of the SMA pathway. **a** The designed SMA pathway. The SMA pathway consists of three modules: (1) Oxidation module that converts C1 (methanol) into a C1 unit (formaldehyde); (2) Fixation module that converts two C1 units and C4 (erythrose 4-phosphate) into a C6 unit (fructose bisphosphate); and (3) Rearrangement module that converts a C6 unit back into a C4 unit (erythrose 4-phosphate) and output a C2 unit (acetyl-CoA). **b** The screening of ALS. **c** In vitro testing of the SMA pathway. Metabolite and enzyme abbreviations: MeoH, methanol; FALD,

formaldehyde; GALD, glycolaldehyde; E4P, erythrose 4-phosphate; H6P, hexose-6-phosphate; F6P, fructose 6-phosphate; AcP, acetyl-phosphate, AcCoA, acetyl-CoA; MDH, methanol dehydrogenase; GALS, glycolaldehyde synthase; HSA, hexose-6-phosphate aldolase; PHI, hexose phosphate isomerase; FPK, fructose-5-phosphate phosphoketolase; PTA, phosphotransacetylase. Values are shown as mean \pm s. d. from three biological replicates. Source data are provided as a Source Data file.

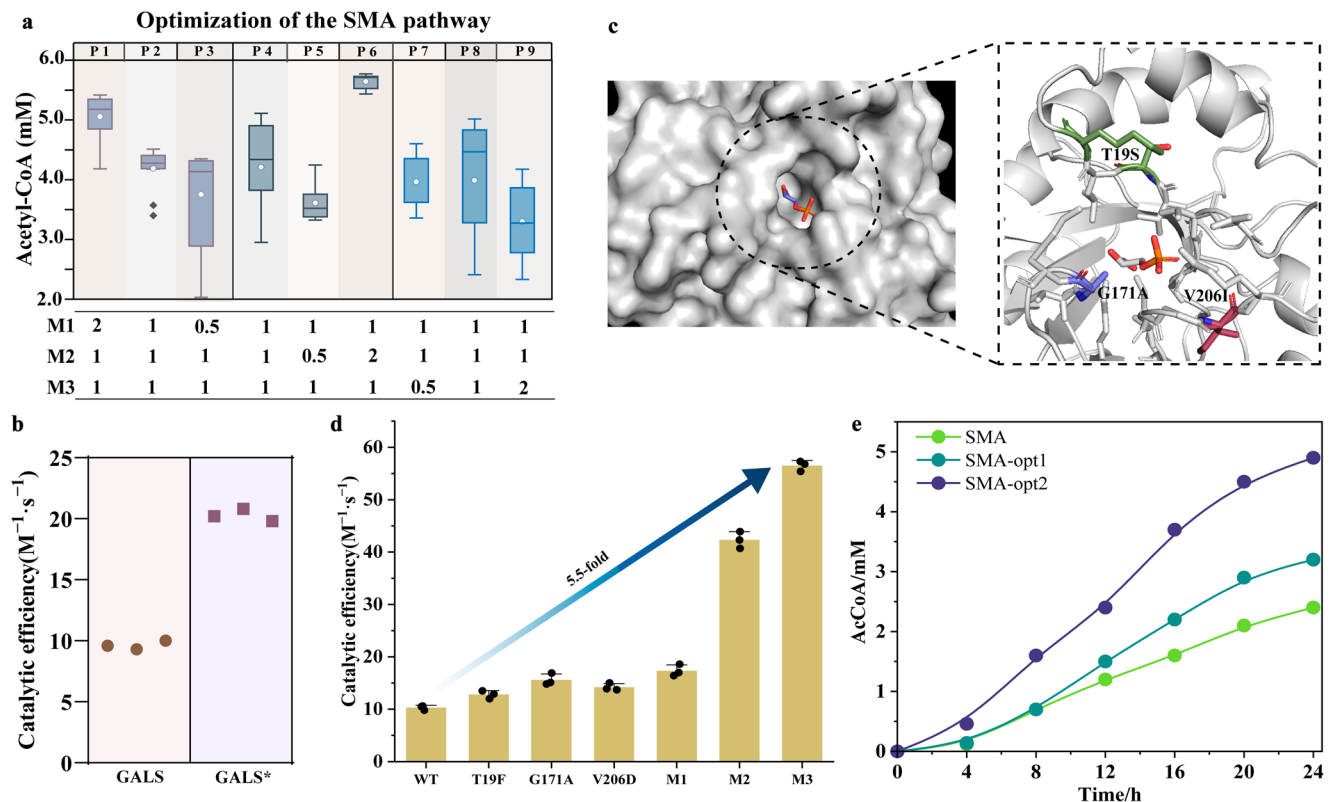


Fig. 2 | Optimization of the SMA pathway. **a** Optimization of the SMA pathway. With each module as the unit of combination optimization, a total of nine different combinations were formed. The box plots showing the minima, maxima, center, bounds of box and whiskers and percentile. **b** Comparison of catalytic activity between GALS and mutant GALS*. **c** Detailed active site view of mutation sites. **d** The catalytic efficiency of WT (*EcDERA*) and its variants for H6P synthesis.

e Acetyl-CoA production rate with GALS* and HSA in the SMA pathway. SMA-opt1 indicated the introduction of GALS*, and SMA-opt2 indicated the introduction of GALS* and HSA. All the experiments were performed in triplicates. Metabolite and enzyme abbreviations: GALS, glycolaldehyde synthase. Values are shown as mean \pm s. d. from three biological replicates. Source data are provided as a Source Data file.

thermodynamically favorable ($\Delta G' < 0$) (Supplementary Table 1, Supplementary Data 1). Second, the Max-min Driving Force (MDF)³⁷ (Supplementary Note 1) was calculated to be 6.12 kJ mol^{-1} , suggesting that the SMA pathway can effectively proceed in the forward direction (Supplementary Fig. 1). Third, the enzyme cost minimization (ECM)³⁸ (Supplementary Note 1) analysis showed that the total protein cost of the pathway enzymes was about 0.55M, excluding the MDH, which demonstrated that high activity towards in the oxidation direction (Supplementary Fig. 2). This result highlighted the potential of the SMA pathway for efficient enzyme protein utilization. Moreover, from an energetic perspective³⁹, this pathway does not consume ATP or/and NAD(P)H, making it an energy-efficient and economical route for methanol assimilation. Lastly, flux balance analysis (FBA)^{40,41} was used to calculate the biomass yield and product acetyl-CoA from synthetic methanol pathways, the SMA pathway has outstanding advantages compared to several others^{15,20,25,34,40} (Supplementary Fig. 3).

To establish the SMA pathway in vitro, a modular construction-assembly-optimization strategy (Supplementary Fig. 4) was employed. In Module I, the *CnMdh* variant CT4-1 (*CnMDH*)³⁶ was selected, demonstrating a catalytic efficiency of $9.3 \text{ M}^{-1}\text{s}^{-1}$ in converting methanol to formaldehyde. In Module II, the engineered *PpGALS* catalyzed the conversion of two molecules of formaldehyde into one molecule of glycolaldehyde³⁴. The third enzyme in module II, *MfPHI*, which catalyze the isomerization of hexose-6-phosphate (H6P) to F6P, was selected and exhibited the highest enzyme activity of 4.7 U/mg (Supplementary Fig. 5)²⁶. With both GALS and PHI in hand, the focus shift on a suitable enzyme for the condensation of glycolaldehyde and E4P to H6P. Based on the catalytic properties related to aldehyde

condensation, 10 native and engineered enzymes were screened (Supplementary Fig. 6). Among these, three candidates exhibited catalytic activity, with deoxyribose-5-phosphate aldolase (*EcDERA*) showing the highest activity, the other seven enzymes did not exhibit this function (Fig. 1b). By incubating GALS, DERA and PHI in a reaction mixture, F6P was synthesized, indicating the successful construction of Module II (Supplementary Fig. 7). In Module III, the conversion rate of F6P catalyzed by *BaFpk* reached 63.7% in the purified enzyme system (Supplementary Fig. 8). *CkPTA* then converted acetyl phosphate into acetyl-CoA as the output product⁴² (Supplementary Fig. 9). The combination of *BaFpk* and *CkPTA* converted F6P to acetyl-CoA (Supplementary Fig. 10).

The SMA pathway was assembled by combining the three modules. Firstly, MDH was added to the reaction system with $100 \text{ mM } ^{13}\text{C}$ -methanol, resulting in the production of ^{13}C -formaldehyde (Supplementary Fig. 11). Further incubation with GALS, DERA and PHI in the reaction mixture led to the detection of ^{13}C -F6P (Supplementary Fig. 12). When ^{13}C -Methanol used as substrate and incubated with purified MDH, GALS, DERA, PHI, FPK and PTA, $2.4 \text{ mM } ^{13}\text{C}$ -acetyl-CoA was synthesized (Fig. 1c). These results confirmed that the SMA pathway was feasible for methanol assimilation to synthesize acetyl-CoA. To identify potential bottlenecks in the SMA pathway, the three metabolic modules was independently regulated. As shown in Fig. 2a, the optimal ratio of pathway enzymes across the three modules was found to be 1:2:1, indicating that module II is the rate-limiting module. In Module II, when the concentration of GALS, DERA or PHI was doubled, the output of this module's product was increased by 3.6, 5.4 or 1.8 times, respectively (Supplementary Fig. 13). These results

demonstrate that GALS and DERA were the rate-limiting enzymes in Module II.

The SMA pathway was subsequently optimized by modifying the rate-limiting enzymes GALS and DERA through protein engineering to enhance pathway efficiency. Using a high-throughput screening method⁷, a high-performance mutant, GALS*(N27S/F397A), was obtained (Supplementary Fig. 14). This variant exhibited a 2.1-fold increase in catalytic efficiency compared to that of GALS (Fig. 2b). Next, efforts were made to alter the substrate preference of *Ec*DERA towards non-natural aldehyde donor glycolaldehyde. All residues surrounding the active center of *Ec*DERA were screened, with 24 sites within 5 Å of the active center selected for single-point saturation mutagenesis (Supplementary Fig. 15a). After screening, three sites were found to have the most beneficial effects (Supplementary Fig. 15b). These mutations were individually introduced into *Ec*DERA, with the G171A showing the highest activity and designated as M1. Through two additional rounds of iterative combinatorial mutagenesis, a highly active mutant, M3 (T19S/G171A/V206I), was obtained and renamed hexose-6-phosphate aldolase (HSA) (Fig. 2c). Compared to the wild type, HSA exhibited a more than 5.5-fold increase in catalytic efficiency (Fig. 2d). By introducing GALS* and HSA into the SMA pathway, the rate of ¹³C-acetyl-CoA production increased by 2.0-fold (Fig. 2e).

Rational design and laboratory evolution for obtaining synthetic methylotroph

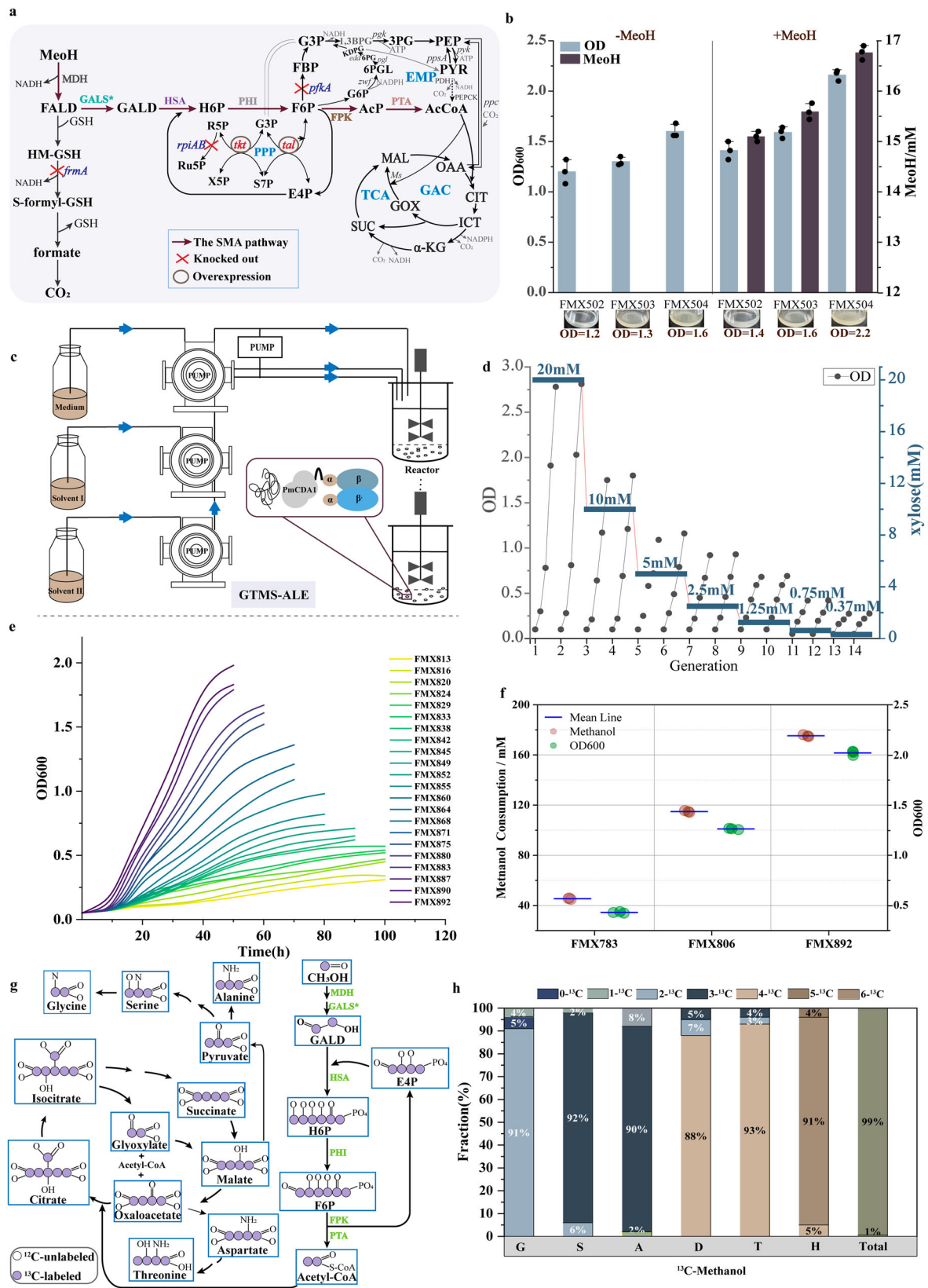
The SMA pathway was introduced into *E. coli* FMX501 (BW25113Δ*frmA*) using three plasmids in a modular manner, resulting in the creation of strain FMX502 (Fig. 3a and Supplementary Fig. 4). However, the optical density at 600 nm (OD₆₀₀) of strain FMX502 was 1.4 in NBS medium with 500 mM methanol and 10 mM xylose (NBS-MX), indicating limited growth compared with xylose as carbon source (NBS-X) (OD₆₀₀ = 1.2) (Fig. 3b)²⁶. To enhance methanol assimilation, the *pfkA* gene was deleted to weaken the metabolic flux of F6P into the glycolytic pathway (EMP), resulting in an increased OD₆₀₀ of 1.59 for the strain FMX503. Additionally, the OD₆₀₀ of FMX503 was 1.3 in methanol-free medium (NBS), indicating that the strain had become methanol-dependent. Furthermore, the overexpression of *tkt* (encoding transketolase from *B. methanolicus*) and *tal* (encoding transaldolase from *E. coli*) was employed to promote E4P regeneration and enhance H6P synthesis. This resulting strain FMX504 achieved an OD₆₀₀ of 2.2 in NBS-MX and 1.6 in NBS-X, but was unable to grow in NBS medium containing only 500 mM methanol (NBS-M). To convert strain FMX504 into a methylotrophic *E. coli*, a genome-targeting mutator strategy (GTMS) was employed for a long-term evolution¹³ using the automatic microbial adaptive evolution instrument (EVOL cell) (Fig. 3c). The mutant fusion protein⁴³ (PmCDA1 fused to *E. coli* RNA polymerase) was introduced into strain FMX505 (strain FMX504Δ*ung*, which lacks uracil-DNA glycosylase) to create strain FMX506. The starting strain FMX506 was then evolved in NBS medium with 500 mM methanol and 20 mM xylose²³. The evolutionary pressure was increased by gradually reducing the xylose concentration from 20 mM to 1.25 mM in the feed medium (Fig. 3d). Under these conditions, the OD₆₀₀ of the evolved strain FMX540 reached at 0.68, which was 31.3% higher than that of strain FMX506 (about 0.52) (Supplementary Table 2 and Supplementary Fig. 16). To enable strain FMX540 to grow using methanol as the sole carbon source, the xylose concentration was further reduced to 0 mM over a period of 140 days and 215 passages, resulting in strain FMX783, which achieved an OD₆₀₀ of 0.43 (Supplementary Fig. 17). To further improve intracellular metabolism, additional evolution in micro-vitamin B was conducted. After 110 more passages, strain FMX892 was obtained (Fig. 3e). This methylotrophic *E. coli* consumed 186.4 mM methanol, reaching a final OD₆₀₀ of 2.2, with a yield of 0.15 gDCW/gMeOH and a doubling time of 4.5 h.

The OD₆₀₀ of the evolved strains FMX783, FMX806, and FMX892 was found to positively correlated with methanol consumption, suggesting that these strains were synthesizing biomass from methanol (Fig. 3f). To confirm that all metabolic products were derived from methanol, ¹³C-methanol labeling experiments were conducted, and the labeling pattern of proteinogenic amino acids was analyzed using liquid chromatography-mass spectrometry (LC-MS). As shown in Figs. 3g, h, the labeling of relevant central-metabolites and amino-acids confirmed the activity of the SMA pathway. Specifically, pyruvate, indicated by the labeling of alanine, was predominantly three-carbon-labeled. This labeling pattern was consistent with the synthesis of pyruvate from two molecules of ¹³C-acetyl-CoA and the release of one molecule of CO₂ via the glyoxylate shunt. The labeled ¹³C-pyruvate is produced from oxaloacetate (OAA) during its formation from acetyl-CoA, as indicated by the ¹³C labeling pattern in aspartate. In addition, the carbon labeling of threonine, derived from OAA, indicated carbon flux through the reductive tricarboxylic acid (TCA) cycle²⁵. As predicted, quadrupled labeled threonine confirmed that the flux of reductive TCA cycle was higher than that through the oxidative TCA cycle, highlighting the reductive TCA cycle as an efficient carbon sequestration pathway for assimilating methanol to synthesize cell growth precursors. Furthermore, ¹³C-labeled serine (derived from 3-phosphoglyceraldehyde) and histidine (derived from ribose-5-phosphate) were detected. This labeling confirmed that this methylotrophic *E. coli* possessed a complete set of enzymes necessary for methanol assimilation, carbon fixation, and operation of the TCA cycle. Finally, when fed with ¹³C-methanol, nearly all relevant amino acids were labeled, and the total proportion of labeled carbon reached at 99.4%. These data indicated that the SMA pathway was constructed in *E. coli*, with biomass carbon derived solely from methanol.

TRCs prolong the doubling times in synthetic methylotrophs

The doubling times of strains FMX506, FMX783 and FMX892 at different evolutionary stages were calculated to be 79.2 h, 56.1 h, and 4.5 h, respectively (Fig. 4a). Additionally, the cell mortality rates of these strains were 41.2%, 33.9% and 17.3%, respectively (Supplementary Fig. 18). Based on these differences, it was assumed that excessive formaldehyde accumulation in the pro-evolutionary strains²⁷ might be responsible. However, the results showed that the formaldehyde content of strain FMX892 was below the detectable limit, and the intracellular formaldehyde levels in strain FMX506 and FMX783 were 135 μM/OD and 98 μM/OD, respectively, both well below the lethal threshold (250 μM/OD), thereby ruling out this assumption (Fig. 4a).

To explore the molecular mechanisms influencing that determined doubling time in synthetic methylotrophs, tritiated thymidine (³H-thy) was incorporated into the trichloroacetic acid-precipitable fraction⁴⁴, revealing that the DNA replication rate in strain FMX783 was 8.9 times lower than in strain FMX892 (Fig. 4b). As illustrated in Figs. 4c, d, further analysis using DAPI staining⁴⁵ to visualize total DNA molecules showed an 8.7-fold difference in fluorescence intensity between strain FMX783 and FMX892, indicating a direct linear relationship between prolonged doubling time and reduced DNA replication rate. In *E. coli*, transcription and DNA replication occur simultaneously on the same DNA template, which can lead to transcription-replication conflicts (TRCs)^{44,46}. To investigate whether TRCs were causing the observed compromised DNA replication, 0.1 mM of the transcription elongation inhibitor rifampicin was added. DNA replication in strain FMX783 was significantly improved by this treatment, increasing DNA content by 4.9 folds. In contrast, the wild type (WT) and strain FMX892 showed only slight increases of 0.2-folds and 1.3 folds, respectively (Figs. 4e, f). To further confirm the presence of TRCs, RNA polymerases (RNAPs) β'Δ(V1204-R1206)⁴⁷ were introduced into the three strains to alter the transcription rate. The resulting strain FMX783R1 showed a shortened doubling time, while no significant changes were observed in strain WTR1 and



FMX892R1 (Supplementary Fig. 19). In addition, the *dnaA*(Sx) allele (*dnaA*^{A213D/R423L/T435K})⁴⁸ was introduced to reduce TRCs by decreasing DNA replication initiation, obtaining strains WTD1, FMX783D1 and FMX892D1. The doubling time of strain FMX783D1 and FMX892D1 was shortened by 18.9 h and 0.6 h, while strain WTD1 remained essentially unchanged (Supplementary Fig. 20). These results

suggested that the aggravation of TRCs contributed to the prolonged doubling time observed in the early evolutionary strain.

To rule out the possibility of GTMS causing TRCs, PMCDA was removed from strain FMX783 (FMX783 PMCDA-) and its DNA replication rate and doubling time were measured. As expected, they were essentially unchanged from FMX783 (Supplementary Fig. 21). To

Fig. 3 | Rational design and directed evolution for obtaining synthetic methylotroph. **a**, Scheme of the rational design for enhancing methanol assimilation in *E. coli*, by introducing SMA pathway, blocking methanol dissimilation and strengthening E4P regeneration. **b**, The cell growth and methanol assimilation in rationally engineered strains. **c**, Adaptive evolutionary genome-targeting mutants (GTMS-ALE) for methanol assimilation. **d**, The OD₆₀₀ of representative evolved strains by gradually decreasing xylose concentration from 20 mM to 0.375 mM. **e**, The growth curve of methylotrophic strain from FMX783 to FMX892. **f**, OD₆₀₀ and methanol assimilation of methylotrophic strains FMX783, FMX806 and FMX892. **g**, Labeling pattern of proteinogenic amino acids on feeding with ¹³C-methanol. It was the ¹³C-labeling schematic diagram. **h**, The proportion of the ¹³C atom label. All **b**, **f**, Data are presented as mean values ± SD, n = 3 independent biological experiments. Metabolite and enzyme abbreviations: G3P, glyceraldehyde 3-phosphate; PYR, pyruvate; PEP, Phosphoenolpyruvate; OAA, oxaloacetate; α-KG, α-ketoglutarate; SUC, succinate; CIT, citrate; R5P, ribose 5-phosphate; X5P, xylulose 5-phosphate; Ru5P, ribulose 5-phosphate; FBP, fructose biphosphate; S7P, sedoheptulose 7-phosphate; HM-GSH,

hydroxymethyl glutathione; S-formyl-GSH, S-formylglutathione; MeOH, methanol; FALD, formaldehyde; GALD, glycolaldehyde; E4P, erythrose 4-phosphate; H6P, hexose-6-phosphate; F6P, fructose 6-phosphate; AcP, acetyl-phosphate, AcCoA, acetyl-CoA; MDH, methanol dehydrogenase; GALS, glycolaldehyde synthase; HSA, hexose-6-phosphate aldolase; PHI, hexose phosphate isomerase; FPK, fructose-5-phosphate phosphoketolase; *frmA*, glutathione dehydrogenase; *rpiA*, ribose-5-phosphate isomerase A; *rpiB*, ribose-5-phosphate isomerase B; *tkt*, transketolase; *tal*, transaldolase; *gnd*, phosphogluconate dehydrogenase; *pyk*, pyruvate kinase; *ppc*, phosphoenolpyruvate carboxylase; *ppsA*, phosphoenolpyruvate synthetase; PTA, phosphotransacetylase. Pathway abbreviation: PPP, pentose phosphate pathway; EMP, Embden-Meyerhof-Parnas; TCA, tricarboxylic acid cycle; ED, Entner-Doudoroff; GCA, Glyoxylate cycle. Annotations: GTMS-ALE, adaptive evolutionary of genome-targeting mutants, RNAP, *E. coli* RNA polymerase, α/β, α/β-subunit of *E. coli* RNA polymerase, PmCDAI, Cytidine deaminase. Amino acid abbreviations: G, Glycine; S, Serine; A, Alanine; D, Aspartate; V, Valine; T, Threonine; H, Histidine. Source data are provided as a Source Data file.

investigate the reason for aggravated TRCs in early evolutionary *E. coli*, *GreA*, *DksA* and *Mfd*, which interact with RNAPs secondary channel to prevent RNAPs stalling^{44,49,50}, were individually knocked out. Meanwhile, ethynyl-uridine (EU) labeling was used to track the newly synthesized RNA⁵¹, revealing that the deletion of these genes reduced RNA synthesis to varying degrees (Figs. 5a–c). In addition, knockout of these genes in strain FMX783 prolonged their doubling times without affecting WT (Fig. 6a). These findings demonstrated that RNAP stalling contributed to TRCs in early evolutionary methylotrophs. It was hypothesized that RNAPs stalling was caused by excessive negative DNA supercoiling, which also led to the accumulation of R-loops structures formed between nascent mRNA and double-stranded DNA⁵². To test this hypothesis, the accumulation of R-loops in strains FMX783 and FMX892 was examined using the S9.6 antibody, which specifically detect DNA: RNA hybrids⁵³. As anticipated, the amount of DNA: RNA hybrids in strain FMX783 increased by 12.8-fold compared to strain FMX892, indicating an excessive negative supercoiling state in early evolutionary *E. coli* (Fig. 6b).

To further examine whether the accumulation of R-loops affected cell growth in synthetic methylotrophs, the *rnhA* gene, which encode RNase HI⁵⁴, was knocked out. The doubling time of strain FMX783Δ*rnhA* was prolonged by 10.4 h (Fig. 6c). In contrast, overexpression of *rnhA* shortened the doubling time of strain FMX783*rnhA*⁺ by 8.7 h. Additionally, overexpression of the bacteriophage T4 UvsW helicase, which unwinds DNA: RNA hybrids. The doubling time of strain FMX783UvsW⁺ was shortened by 12.5 h, and the amount of DNA: RNA hybrids was reduced to 57.1% (Supplementary Fig. 22). Furthermore, knocking out *rnhA* in strain FMX892 prolonged the doubling time by 16.9 h. Overexpression of *rnhA* and UvsW in this strain shortened the doubling times by 0.5 h and 0.3 h, respectively (Supplementary Fig. 23). Together, these data indicated that excessive negative DNA supercoiling led to RNAPs stalling and the accumulation of R-loops in early evolutionary *E. coli*, resulting in prolonged cell doubling time (Fig. 6d).

TOPAI regulates EcTopoi-RNAPs association to relieve TRCs

To explore the changes in gene expression that facilitated cell growth in methanol during evolution, genome sequencing analysis was conducted on the starting strain FMX506 and two evolved strains, FMX783 and FMX892 (Supplementary Table 3). Compared to strain FMX506, the evolved strains FMX783 and FMX892 exhibited common mutations in *uspB* (encoding universal stress protein B), *emry* (encoding multidrug resistance protein) and *geneO833* (encoding sigma-54-dependent Fis family transcriptional regulator) (Fig. 7a). In addition, both the evolved strains shared mutations in *rlmF* and *folk* (encoding methyltransferases involved in tetrahydrofolate synthesis). Other observed genetic changes included the insertion sequence IS3,

truncation of *fbab* (encoding fructose-bisphosphate aldolase) and copy number variation of TOPAI (TopA inhibitor). Reverse metabolic engineering experiments revealed that these genetic changes improved the cell growth rate of strain FMX783 on methanol (Fig. 7b). Specially, the *uspB*^{V60E} mutation increased the growth rate by 9.8%, while the *emry*^{M119I} mutation did not result in any improvement. The *rlmF*^{F289V} and *folk*^{N121T} mutations increased the growth rate by 5.7% and 8.3% respectively, suggesting a reduction in the spontaneous reaction between tetrahydrofolate and formaldehyde, thereby channeling more formaldehyde into the SMA pathway⁵⁵. Furthermore, the *geneO833*^{Q281K} mutation alleviated DNA-binding transcriptional repression, leading to a 7.2% increase in growth rate. The truncation in *fbab*^{*}(Δ213–229) reduced the downstream shunt of F6P, thereby strengthening the synthetic assimilation cycle. Moreover, the IS3 family transposase was inserted upstream of the 3'-5' exoribonuclease, but it did not have any growth improvement. The copy number of TOPAI gene was doubled in strain FMX783, while it was truncated in the evolved strain FMX892. Confirmatory experiments showed that overexpression of TOPAI in strain FMX783 (FMX783T1) reduced the cell growth rate by 36.3%. Conversely, deletion of TOPAI (FMX783T2) significantly restored cell growth (Fig. 7c, d).

To explore the regulatory mechanism behind the shortened doubling time, whole-transcriptome analysis was conducted on three evolved strains. Compared with the starting strain FMX506, 453 upregulated genes and 1367 downregulated genes were identified in strain FMX783, and 495 upregulated genes and 1649 downregulated genes were identified in strain FMX892 (Supplementary Fig. 24). When comparing strain FMX892 to strain FMX783, 18 genes were up-regulated and 120 were down-regulated. Within the SMA pathway, the expression of *mdh* was significantly up-regulated, and genes *atoA*, *atoB*, *atoD* and *atoE*, involved in acetyl-CoA transport, were up-regulated by 7.9-, 8.1-, 10.7- and 8.5-fold in strain FMX892, respectively (Fig. 7e). Meanwhile, the expression of the *citC* gene, associated with the TCA cycle, expression was down-regulated by 3.5-fold, indicating a weakening of the TCA cycle in the evolved strain FMX892. In addition, the *pyk* gene of ATP synthesis and the *zwf* gene of NADPH regeneration were up-regulated by 3.0 and 2.2 times, respectively, suggested that energy synthesis was critical for cell growth in synthetic methylotrophs. Gene Ontology (GO) analysis revealed that differentially expression genes (DEGs) across three branches-biological processes (BP), cell components (CC) and molecular functions (MF), were involved in transcription-replication conflicts (TRCs) (Supplementary Fig. 25). To identify key genes regulating TRCs, the transcription levels of relevant genes were further analyzed, revealing significantly differences in the expression of TOPAI, *YjhQ*, *dicC*, *alpA* and *hycA* (Supplementary Fig. 26). RT-PCR analysis confirmed that mRNA levels of *dicC*, *alpA*, *hycA* and TOPAI were decreased by 2.3-, 1.6-, 0.9- and 3.7-fold,

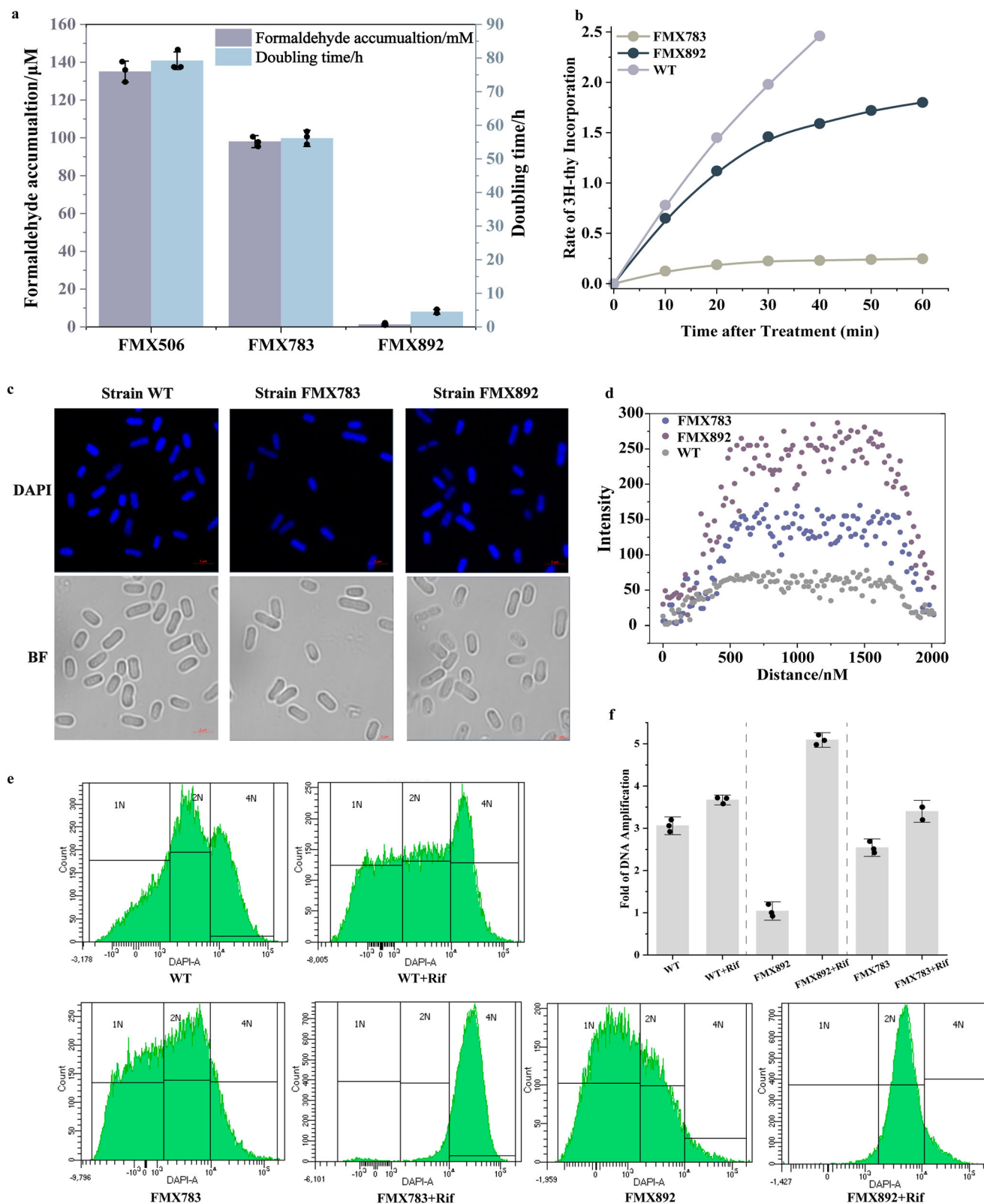


Fig. 4 | TRCs prolong doubling times in synthetic methylotrophs.

a Formaldehyde accumulation and the doubling times of evolved strains FMX506, FMX783 and FMX892. **b** Rate of ^3H -thy incorporation in strains WT, FMX783 and FMX892. **c** Characterization of DNA content in strains WT, FMX783 and FMX892. It showed fluorescence imaging and bright field images of DAPI-labeled DNA. Three times each experiment was repeated independently with similar results.

d Quantification of cell fluorescence intensity in DNA content using ImageJ. **e** DNA replication integrity of strains WT, FMX783 and FMX892 incubating with rifampicin. **f** Statistical analysis of DNA replication integrity in strains WT, FMX783 and FMX892 added rifampicin. All (**a**, **f**) Data are presented as mean values \pm SD. $n = 3$ independent biological experiments. Source data are provided as a Source Data file.

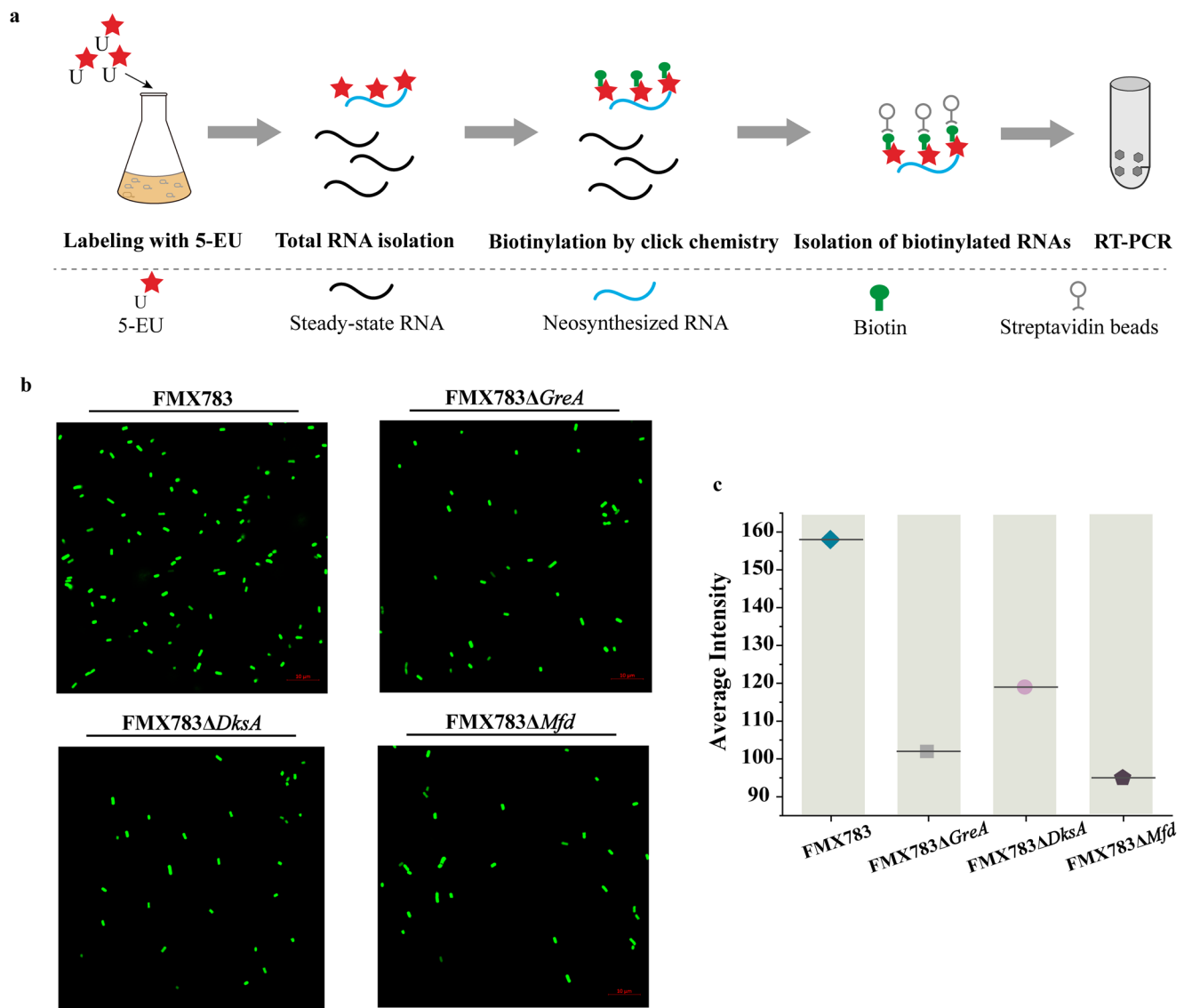


Fig. 5 | RNAPs stalling aggravated the occurrence of TRCs. a EU-labeled RNA content determination. It is flow chart of the experimental procedure for EU-labeled nascent RNA. **b** The EU-labeled new RNA in strains FMX783, FMX783 Δ GreA, FMX783 Δ DksA, and FMX783 Δ Mfd captured by laser scanning confocal microscope.

c Quantification of cell fluorescence intensity in EU-labeled RNA content using ImageJ. Three times each experiment was repeated independently with similar results. Source data are provided as a Source Data file.

respectively, while *YjhQ* expression level increased by 3.1-fold (Fig. 7f). Combined with the copy number variation of TOPAI in the genome sequencing data, it is suggested that, TOPAI may play a critical role in regulating TRCs, thereby determining the doubling time of synthetic methylotrophs.

To test this hypothesis, the TOPAI gene was either deleted or overexpressed in strain FMX783, obtaining the strains FMX783-TOPAI⁺ (FMX783T1) and FMX783- Δ TOPAI (FMX783T2), respectively. The mortality rates for strains FMX783T1 and FMX783T2 were 49.5% and 22.7%, respectively. The doubling time of strain FMX783T2 was shortened by 33.6 h compared to strain FMX783, whereas the doubling time of strain FMX783T1 was extended by 29.4 h (Fig. 8a). Additionally, the overexpression of TOPAI in strain FMX892, resulting in strain FMX892T1, extended the doubling time by 39.7 h (Supplementary Fig. 27). To further investigate, *YjhQ* was co-expressed with TOPAI in strain FMX783, creating strain FMX783Y1, because *YjhQ* forms a toxin-antitoxin (TA) system with TOPAI in *E. coli*⁵⁶. The cell mortality of FMX783Y1 decreased to 28.1%, without affecting WT (Figs. 8a and

Supplementary Fig. 28), suggesting that TA system plays a significant role in the survival of synthetic methylotrophs. However, the doubling time, remained unchanged.

Next, the role of TOPAI in regulating the doubling time of these synthetic methylotrophs was explored. Co-IP (Co-Immunoprecipitation) and BiFC (bimolecular fluorescence complementation) experiments identified EcTopol was that target protein of TOPAI in strain FMX783 (Fig. 8b). When 2.5 μ g/mL chloroquine was added, the compact DNA migration accelerated in cells overexpressing TOPAI, and an excess of negatively supercoiled DNA appeared within 10 min after TOPAI expression in strain FMX783T1, indicating that TOPAI binding to EcTopol induced hyper-negative supercoiling (Fig. 8c). Further investigation using the same BiFC techniques confirmed the physical interaction of EcTopol and RNAPs⁵² (Supplementary Fig. 29). Chromatin Immunoprecipitation (ChIP) combined with RT-PCR⁵⁷ was then used to quantify the binding rate of EcTopol and RNAPs in promoter region, showing rates of 20.7% in strain FMX783T1 and 36.9% in strain FMX783T2 (Supplementary Fig. 30). These data suggested that TOPAI

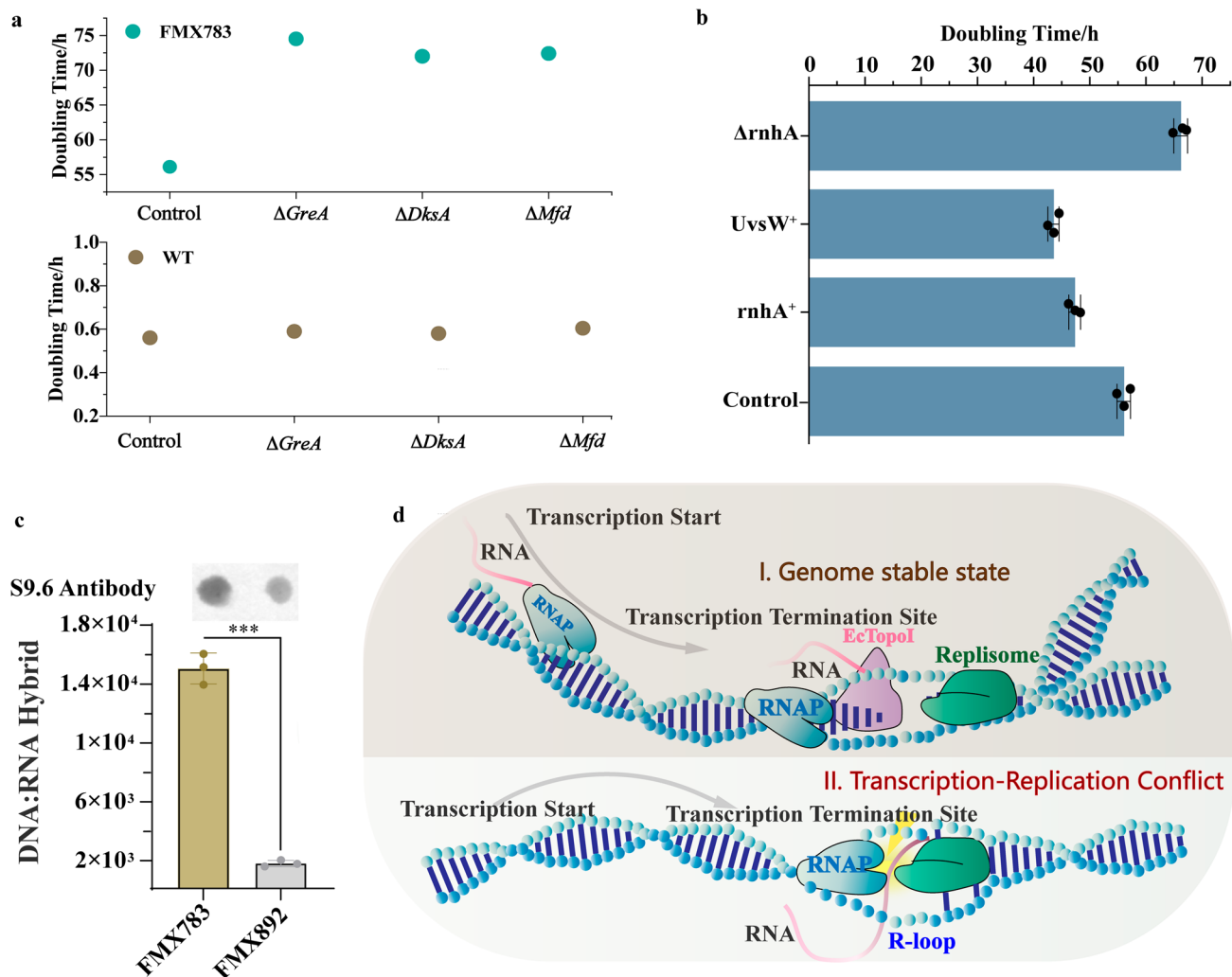


Fig. 6 | RNAPs stalling aggravated the occurrence of TRCs. a The effect of deletion of gene *GreA*, *DksA* and *Mfd* in strains WT and FMX783 on doubling times. **b** The DNA-RNA hybrid of evolved strains FMX783 and FMX892. **c** The effect of knockout of DNA: RNA hybrid regulatory genes on the doubling time of strain FMX783. Significance (P -value) was evaluated by two-sided t-test. Significant

differences were marked as $*P < 0.05$, $**P < 0.01$ and $***P < 0.001$. **d**, RNAPs stalling aggravated TRCs and R-loops accumulation. The model showed how RNAPs stalling and R-loops accumulation were caused during the normal growth phase as well as when TRCs occurred. All **b**, **c**, Data are presented as mean values \pm SD, $n = 3$ independent biological experiments. Source data are provided as a Source Data file.

inhibited EcTopol activity and limited its binding to RNAPs, leading to the uncoupling of EcTopol-RNAPs in early evolutionary *E. coli*.

The results demonstrated that TOPAI interaction with EcTopol led to excessive negative supercoiling. The promoter binding rates of EcTopol and RNAPs in WT, FMX783 and FMX892 were measured, which were 37.9%, 18.4% and 31.5%, respectively (Fig. 8d). In strain FMX783T1 and FMX783T2, these binding rates were 20.7% and 36.9%, respectively, further confirming that TOPAI acting on EcTopol disrupted the RNAP: EcTopol interaction in early evolutionary methylotrophs. To further investigate the uncoupling of the RNAP-EcTopol interaction in strain FMX892, the CTD (a 14 kDa RNAP-binding EcTopol C-terminal domain) was overexpressed in strain FMX892 (FMX892U1), introduced an inactive mutant EcTopol Y319F (FMX892U2), and deleted the EcTopol domain topA Δ 30⁵² (FMX892U3). These modifications led to a decrease in promoter binding rates of EcTopol and RNAPs by 10.5%, 12.7% and 14.3%, respectively, bringing them closer to the binding rate observed in FMX783, while having minimal effect on WT (Supplementary Fig. 31). It was also observed that DNA migration rates in the three strains, after uncoupling, were significantly accelerated compared to strain FMX892 (Supplementary Fig. 32). In addition,

R-loops accumulation increased by 27.9%, 31.8% and 26.5% in the three strains, respectively (Supplementary Fig. 33). These findings indicated that the uncoupling of RNAP: EcTopol interaction led to excessive negative supercoiling, resulting in R-loops accumulation. Furthermore, the EU signal intensity for nascent RNA synthesis in strain FMX892 was 35.9% higher than in strain FMX783 (Fig. 8e). Notably, specific labeling of total RNAPII in strains FMX783 and FMX892 revealed no significant difference, ruling out the amount of RNAPII as the primary factor causing TRCs (Supplementary Fig. 34). To confirm the universality of this mechanism, TOPAI was knocked out in the early evolutionary strain FMX795 and over-expressed TOPAI in the late evolutionary strain FMX869. As expected, this led to a shortening of the doubling time by 12.8 h in strain FMX795 and a prolongation by 23.5 h in strain FMX869 (Supplementary Fig. 35). Taken together, TOPAI-mediated inactivation of EcTopol uncoupled it from RNAPs, leading to excessive negative supercoiling, resulting in R-loops accumulation and RNAPs stalling, which aggravated TRCs and prolonged doubling times in synthetic methylotrophs. As evolution progressed, the deficiency of TOPAI alleviated TRCs, allowing strain FMX892 to grow normally using methanol as the sole carbon source.

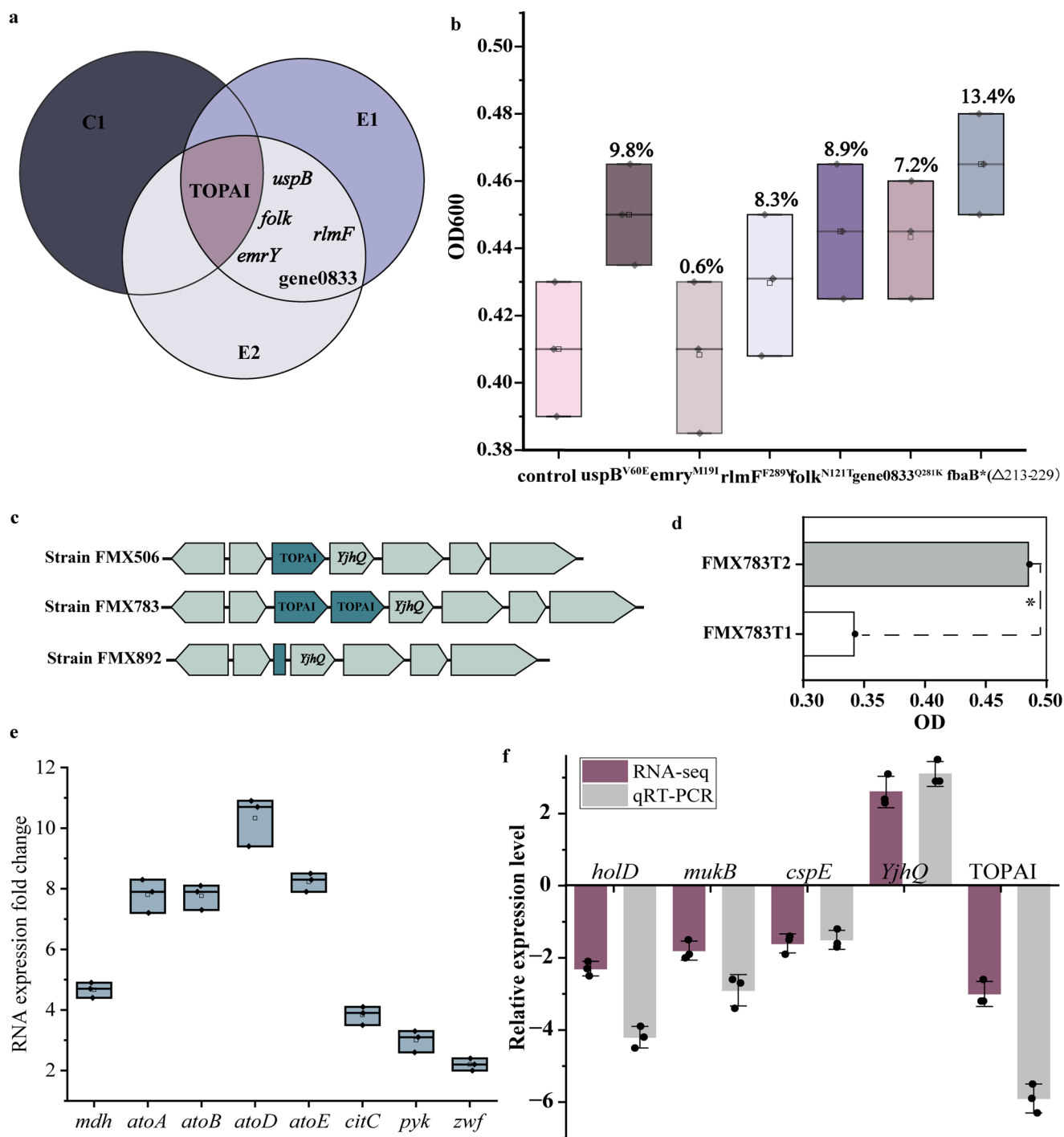


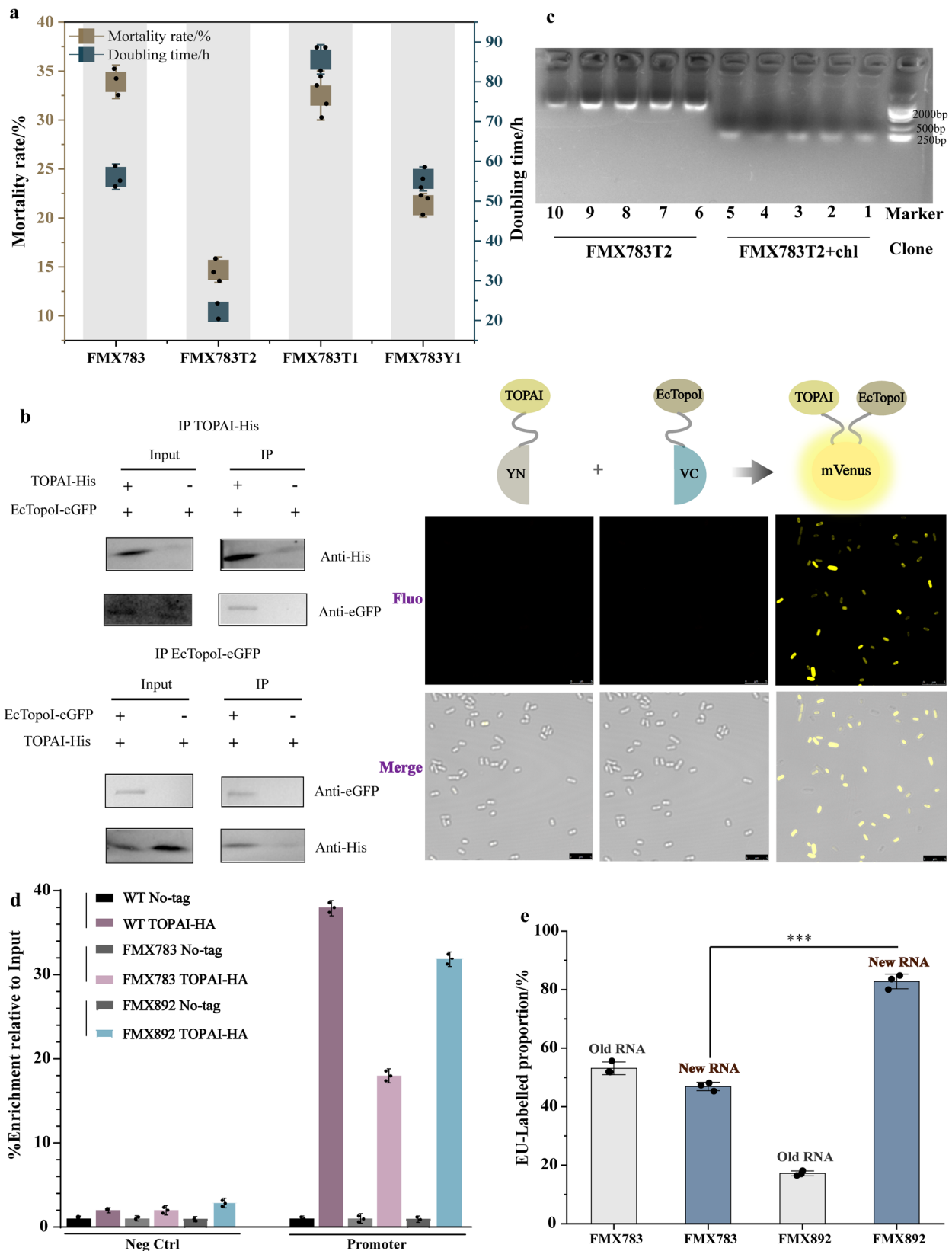
Fig. 7 | Genomic and transcriptome sequencing analysis of synthetic methylotrophs. **a** Common mutations detected using genome sequencing from three strains. C1 represented to the starting strain FMX506, E1 represented to the evolved strain FMX783, and E2 referred to the evolved strain FMX892. Six mutated genes were identified, among which a DNA topoisomerase I inhibitor gene TOPAI was the key mutation. **b** Cell growth by introducing mutations to strain FMX783. The box plots showing the minima, maxima, center, bounds of box and whiskers and percentile. **c** Variation of gene TOPAI in three evolved strains. TOPAI gene existed in

different forms in strains FMX506, FMX783 and FMX892. **d** The effect of TOPAI expression on cell growth of strain FMX783. **e** Transcriptional up-regulation levels of genes *mdh*, *atoA*, *atoB*, *atoD*, *atoE*, *citC*, *pyk* and *zwf*. The box plots showing the minima, maxima, center, bounds of box and whiskers and percentile. **f** mRNA levels of *hold*, *mukB*, *cspE*, *YjhQ* and TOPAI genes. Strain abbreviation: E1, FMX506; C1, FMX783; C2, FMX892. All (**b**, **e**, **f**). Data are presented as mean values \pm SD, $n = 3$ independent biological experiments. Source data are provided as a Source Data file.

Discussion

In this study, an efficient SMA pathway, which required six enzymes to synthesize acetyl-CoA from methanol without the need for ATP or NAD(P)H, was designed and connected to central carbon metabolism. Following the introduction of the SMA

pathway into *E. coli*, a combination of rational design and GTMS-adaptive evolution was used to develop synthetic methylotrophs. Genome and transcriptome sequencing confirmed that, alleviating TRCs improved cell growth and shortened doubling time in methylotrophic *E. coli*. This study provides some valuable



guidance for the future design and application of synthetic methylotrophs.

Designing of a short-step, carbon-neutral and energy-saving methanol assimilation pathway can significantly advance the development of a low carbon economy. Firstly, traditional metabolic engineering has primarily focused on introducing natural methanol

assimilation pathway, such as the serine cycle, into model microorganisms. However, this pathway involves a 17-step enzymatic reaction, reducing the assimilation efficiency⁵⁸. In contrast, the SMA pathway developed in this study requires only six enzymes to synthesize acetyl-CoA from methanol, making it a more efficient assimilation route. In the SMA pathway, protein-engineered HSA catalyzes

Fig. 8 | TOPAI regulating EcTopol-RNAPs association to relieve TRCs. **a** The cell mortality and doubling time of strains FMX783T1, FMX783T2 and FMX783Y1. The box plots showing the minima, maxima, center, bounds of box and whiskers and percentile. **b** Co-IP and BiFC experiments were conducted to verify that TOPAI combined with EcTopol. BiFC system consisting of YN155 (amino acid positions 1–155 in Venus, where amino acid position 65 is mutated from F to L, a point mutation that promotes the maturation of fluorescent proteins) and VC156 (amino acid positions 156–239 in Venus). **c** The supercoiling of strain FMX783T2 (FMX783-TOPAI*) by adding 2.5 µg/mL chloroquine. **d** Association of TOPAI with the core

promoter of RNAP was determined by ChIP analysis and RT-PCR to measure occupancy. **e** EU-labeled old RNA and new RNA of strains FMX783 and FMX892. Abbreviations: FMX783T1, FMX783-ΔTOPAI; FMX783T2, FMX783-TOPAI*; FMX783Y1, FMX783-*YjhQ**, Co-IP, Co-Immunoprecipitation; BiFC, bimolecular fluorescence complementation; EcTopol, Topoisomerase I of *E. coli*. Significance (*P*-value) was evaluated by two-sided *t*-test. Significant differences were marked as **P* < 0.05, ***P* < 0.01 and ****P* < 0.001. Values are shown as mean ± s. d. from three biological replicates. Source data are provided as a Source Data file.

an aldehyde condensation reaction between glycolaldehyde and E4P to produce H6P. This enzymatic reaction opens a new channel from methanol intermediates to central carbon metabolites, offering innovative approaches for the artificial design of carbon rearrangement pathway. Secondly, the RuMP pathway, known for its high assimilation efficiency, has been used in constructing synthetic methylotrophs⁵⁹. Similarly, the XuMP pathway was a unique assimilation route in methylotrophic yeast⁶⁰. However, both the RuMP and XuMP pathways all release CO₂, thereby reducing carbon yield. In this study, a resource-efficient and environmentally friendly SMA pathway was designed and constructed using a modular construction-assembly-optimization strategy. Unlike the RuMP or XuMP pathways, the SMA pathway can achieve carbon neutrality under certain conditions, with no carbon emissions. Thirdly, the Calvin cycle, although it fixes CO₂ and avoids carbon loss, but consumes ATP and NADPH⁶¹. The SMA pathway, by contrast, is an energy-saving carbon assimilation route that does not require reducing power or energy. The central metabolism of host strains is highly plastic, providing a robust framework for the introduction of metabolic pathway⁶². This efficient SMA pathway is a crucial step toward developing synthetic methylotrophs with accelerated cell growth rate.

Synthetic methylotrophs utilizing artificially designed assimilation pathway demonstrate high methanol utilization efficiency and shortened doubling time, overcoming the limitations breaking of natural methylotrophs in chemicals production. Recent research has primarily focused on the relatively simple RuMP cycle²³, which can be introduced into model microorganisms to create methylotrophs. Although extensive efforts have been made to engineer the RuMP pathway in *E. coli*²¹, the transplanted pathway has struggled with lower methanol utilization rates. To enhance methanol assimilation, different metabolic engineering strategies have been employed, including the co-utilization of carbon source substrates, increasing precursor supply and regulating reducing equivalent^{13,17,63}. Recent breakthrough in the RuMP pathway reduced the doubling time to 4.3 hours⁶⁴ and even up to 3.5 h⁶⁵, which is comparable to the doubling time of natural methylotrophs such as *Methylobacterium extorquens* AM1 with a doubling time of 4 h⁶⁶. However, most currently developed synthetic methylotrophs rely on the RuMP pathway for methanol assimilation. To overcome the growth limitations associated with this pathway, an artificially designed SMA pathway was introduced into host strain *E. coli*, resulting in methanol-dependent *E. coli* through metabolic modification. After long-term adaptive evolution, an artificial methylotroph was obtained, achieving an OD of 2.2 and a doubling time of 4.5 h, closely matching the growth performance of natural methylotrophs.

The mechanism by which alleviating TRCs shortens the doubling time of synthetic methylotrophs is expected to facilitate the industrial application of C1 compounds as raw material for bio-refinery process. Synthetic methylotrophs inherently disrupt the original metabolic regulation of the chassis, requiring the integration of different reactions with endogenous metabolism to establish a new metabolic balance. Therefore, a deeper understanding of the cell growth mechanism in synthetic methylotrophs could offer valuable insights for their future application. Recent studies have reported several mechanisms involved in synthetic methylotrophs, primarily focusing on reducing

formaldehyde toxicity in vivo²⁴, regulating cell membrane damage repair²⁷, alleviating DNA-protein crosslinking, and balancing metabolic flux²⁶. Contrary to these mechanisms, this study identified TRCs as the primary factor contributing to the prolonged doubling time in synthetic methylotrophs. Through combination of omics sequencing analysis and validation through reverse metabolic engineering, it was demonstrated that the overexpression of the TOPAI gene caused the uncoupling of EcTopol from RNAPs, which in turn caused the accumulation of R-loops and stalling of RNAPs, thereby aggravating TRCs in strain FMX783. Evolutionary processes eventually mitigated this deficiency in TOPAI, alleviating potential TRCs, and restoring the normal growth rate of strain FMX892 on methanol. Future research will aim to prevent the uncoupling EcTopol from RNAP to inhibit the excessive accumulation of R-loops, thereby alleviating TRCs and progressively enhancing the growth of synthetic methylotrophs. It was hypothesized that the alteration in TOPAI may be directly related to the assimilation of methanol or formaldehyde in early evolutionary strains, this hypothesis needs to be investigated in future work. Overall, this study provides critical guidance for breaking the cell growth limitations in C1-assimilating microorganisms.

Methods

Strains and plasmids

All strains, plasmids, codon-optimized genes and primers used were listed in Supplementary Data 2–5. *E. coli* JMI09 was used as host strain to construct all plasmids. *E. coli* BL21(DE3) and plasmid pET28a were used for overexpression of MDH, GALS*, HSA, PHI, FPK and PTA, which were further used for protein purification. Three synthetic plasmids involving pEM, pCDR and pJO1 were used to express heterologous proteins of the SMA pathway in *E. coli* BW25113. The plasmid pEM and pCDR were constructed by replacing the promoter region and multiple cloning enzyme cleavage sites in pETM6 and pCDM4 with the promoter region and multiple cloning enzyme cleavage sites from pQE-80I-kan, respectively. Promoters used for genetic manipulations were listed in Supplementary Table 4. Ampicillin 100 g L⁻¹, Kanamycin 50 g L⁻¹, streptomycin sulfate 20 g L⁻¹ were added to induce gene expression. Strains, plasmids and protein sequences used in this study were listed in Source Data.

Genetic manipulations

To construct the SMA pathway in *E. coli* BW25113, the gene *frmA* (encoding S-(hydroxymethyl) glutathione dehydrogenase) and *pfkA* (encoding 6-phosphofructokinase I) were knocked out using CRISPR-Cas9 system. MDH, PHI, FPK and PTA were codon-optimized and synthesized by Suzhou AZENTA Biotechnology. GALS* and HSA were modified by protein engineering. MDH was inserted into plasmid pJO1, and GALS*, HSA, and PHI were inserted into plasmid pEM. FPK and PTA were inserted into plasmid pCDR. Three recombinant plasmids consisting of the SMA pathway enzymes were transformed into *E. coli* by electroporation. All plasmids were constructed by one-step cloning kit procedure (Vazyme Biotech Co., Ltd), Gibson Assembly with the NEBuilder kit (New England Biolabs) and ligation cloning procedures (Takara Bio, Dalian, China). CRISPR Cas9-mediated genome engineering was applied for gene knockout, and the guide-RNA was predicted by the ATUM gRNA Design Tool

(<https://atum.bio/eCommerce/cas9/input>). The sgRNA sequences used in this study were listed in Supplementary Table 5.

Culture conditions

Lysogeny broth (LB) was used to construct plasmids and strains, containing 5 g L⁻¹ yeast extract, 10 g L⁻¹ peptone from casein and 10 g L⁻¹ NaCl. Terrific broth (TB) was mainly used for protein expression, containing 24 g L⁻¹ yeast extract, 12 g L⁻¹ peptone from casein, 2.31 g L⁻¹ KH₂PO₄, 16.42 g L⁻¹ K₂HPO₄·3H₂O and 4% glycerol. The NBS minimal medium was used for bacterial cultivation consisting of 25.7 mM KH₂PO₄, 28.7 mM for K₂HPO₄, 26.5 mM for (NH₄)₂HPO₄, 1.0 mM MgSO₄·7H₂O, 102 μM CaCl₂·2H₂O, 29.6 μM vitamin B1 and trace elements (9.9 mM FeCl₃, 840.6 μM CoCl₂·6H₂O, 743.7 μM CuCl₂, 959.8 μM ZnCl₂·4H₂O, 1.4 mM NaMnO₄, 808.7 μM H₃BO₃, dissolve in 0.1 M HCl). 0.1 mM IPTG was added to induce pathway enzymes expressions. Methanol was added to culture medium to give a final concentration of 500 mM. Cultures were inoculated into a 100 mL flask containing 25 mL NBS medium at 37 °C, 200 rpm for 12 h. Cell growth was measured at the population level by maximum cell density (OD₆₀₀).

Adaptive laboratory evolution

Long-term evolution was carried out in an automatic microbial adaptive evolution instrument (EVOL cell). The culture temperature was set at 37 °C and the rotating speed was 200 rpm. The original strain *E. coli* FMX506 was spotted on NBS-MX plate, and three colonies were selected and cultivated in NBS-MX liquid medium (a mixture of 20 mM xylose and 500 mM methanol) for 12 h. Three generations were conducted under the same conditions. *E. coli* cells were then transferred to a fresh NBS containing 500 mM methanol and 10 mM xylose with an initial OD₆₀₀ of ~0.05. In addition, 30 μM vitamin B1, 16.7 μM vitamin B and 30.1 mM inducer IPTG were initially added in culture. After cultivation of 12 h, *E. coli* cells were transferred into a fresh NBS-MX containing 500 mM methanol with gradually reduced xylose concentrations (5 mM, 2.5 mM, 1.25 mM, 0.75 mM and 0.375 mM, through 14 generations, respectively). Then, *E. coli* cells were transferred to NBS without xylose for further culture. This initial methylotroph *E. coli* FMX783 was obtained, which grew solely on methanol, with a maximum OD₆₀₀ of 0.43. To improve the utilization of methanol, 12.8 μM vitamin B6, 9.4 μM biotin and 9.1 μM vitamin B5 were also added. Besides, 7.5 mM NaNO₃ was incorporated as an additional electron donor. Finally, the evolved strain *E. coli* FMX892 was obtained with a maximum OD₆₀₀ of 2.2. The growth performance of methanol-dependent and methylotrophic strains was tested every 2-3 generations, and the doubling time of evolved strains was calculated by reference to the standard formula (Supplementary Note 2).

¹³C labeling experiment

For analysis of ¹³C-labeled amino acids and central metabolites, the evolved strains FMX783 and FMX892 were cultured overnight in unlabeled methanol as the sole carbon source and washed twice with PBS (pH = 7.4), and then transferred to ¹³C-labeled methanol (Sigma-Aldrich, MO, USA) as the sole carbon source. This process was repeated five times on labeled methanol, then *E. coli* cells were washed twice with PBS, and finally transferred to fresh ¹³C-labeled methanol as the sole carbon source. *E. coli* cells were cultured to exponential growth stage (OD = 0.5), and then 2 mL cultures were pelleted at 8000 × g, 4 °C for 5 min. After that, *E. coli* cells were resuspended in a cold solution containing 300 μL of -20 °C methanol, 300 μL of -20 °C chloroform, and 250 μL of 4 °C water⁶⁷. The supernatant of metabolite extract was transferred into 1.5 mL Eppendorf tube and freeze-dried at low temperature. Then, dry extract was resuspended in 400 μL acetonitrile: water (54.9:45.1, v/v), ultrasonically broken for 10 min and centrifuged at 12,000 × g and 4 °C for 10 min to remove insoluble

fragments. The supernatant was transferred to an HPLC vial and stored at -80 °C for LC-MS/MS analysis.

Flow cytometry assay

E. coli cells were washed with PBS buffer twice and resuspended to OD₆₀₀ of 0.35. The fluorescence of each sample was measured by BD FACSAria III cytometer (BD Biosciences, the United States). 5-EU-labeled strains were measured in the FITC channel (488 nm EL, 530/30 nm EF) and DAPI strains were measured in the PE-Cy5-A Blue channel (400 nm EL, 450/30 nm EF), whereas PI stains were detected in the PE-Cy5-A Red channel (561 nm EL, 670/14 nm EF). A total of 20,000 *E. coli* cells were used for analysis for each sample. All data was collected by FlowJo software.

Protein purification

Recombinant plasmids for *His6*-MDH, *His6*-GALS*, *His6*-HSA, *His6*-PHI, *His6*-FPK and *His6*-PTA were transformed into *E. coli* BL21(DE3) for protein expression. The cell pellet was resuspended in 30 mL washing buffer (50 mM Na₂HPO₄, 150 mM NaCl, pH 8.0) containing a protease inhibitor and subsequently lysed by high pressure homogenizer⁶⁸. The lysed cells were incubated with DNase I (final concentration 0.1 mg mL⁻¹) for 30 min at 4 °C. After removing cell debris by centrifugation (12857 × g, 30 min, 4 °C). The cleared lysate was loaded on a Strep-Tactin column (Strep-Tactin Superflow high capacity), incubated for 60 min at 4 °C, and the protein was purified according to the manufacturer's guidelines. Proteins were desalted using 10 DG desalting columns (BioRad) with PBS pH 10.0 and analyzed by SDS-PAGE. Protein concentration of purified enzyme was measured by detecting absorbance at 280 nm using a NanoPhotometer N50 spectrophotometer. All purification operations were conducted at 4 °C when necessary.

Liquid chromatograph mass spectrometer

Detection was performed on a Sciex LC coupled to a triple quadrupole trap mass spectrometer (QTRAP 5500, AB Sciex, USA) (Q-TRAPMS) with electrospray ionization (ESI) in negative mode. The HPLC analysis was performed on the BEH C18 column (2.5 μm, 2.1 × 50 mm; Waters) at a temperature of 40 °C. The mobile phase was a mixture of two solvents: A- water (0.1% FA) and B- acetonitrile. The optimized linear gradient system was as follows: 0 min, 95% A; 0–1 min to 95% A; 1–5 min, to 5% A; 5–7 min, 5% A; 7–10 min to 95% A. The autosampler was set to 4 °C. The injection volume was 2 μL, and the flow rate was 300 μL/min. The injection needle was washed after each injection with acetonitrile. The instrument parameters were as follows: ion spray voltage (IS): 5500 V; temperature: 550 °C; nebulizer gas (GS1): 60 psi; turbo gas (GS2): 60 psi; curtain gas (CUR): 35 psi; and collision gas (CAD): medium. Instrument control and data integration were performed using Analyst® Software Version 1.6.2. Sample processing: Protein samples were boiled at 100 °C for 10 min and centrifuged at 14,000 × g for 10 min, the supernatant was collected and filtered through 0.22 μm filter membrane and then determined by LC-MS detection (according to the situation or ethyl acetate appropriate dilution). The total number of sample and control are 1, three times of biological replicates.

Genome sequencing analysis

E. coli strains FMX506 (C1), FMX783 (E1) and FMX892 (E2) were streaked on LB solid medium and cultured at 37 °C for 12 h. Next, a single colony on solid medium was inoculated into 200 mL of LB liquid medium and cultured at 37 °C for -12 h at 200 rpm. *E. coli* cells were harvested after 10 min centrifugation at 12,000 × g. Genomic DNA of C1, E1 and E2 were extracted using Wizard® Genomic DNA Purification Kit (Promega) and quantified by TBS-380 fluorometer (Turner Bio-Systems Inc., Sunnyvale, CA). High quality DNA (OD₂₆₀/280 = 1.8 - 2.0, ≥ 10 μg) was used for genomic sequencing through combination of

PacBio Sequel II and Illumina sequencing platforms. The Illumina data was used to evaluate the complexity of the genome.

Transcriptome analysis

Total RNA was extracted using TRIzol® Reagent according to the manufacturer's instructions (Invitrogen). Then, RNA quality was determined by 2100 Bioanalyser (Agilent) and quantified using the ND-2000 (NanoDrop Technologies). High-quality RNA sample ($RIN \geq 6.5$) was used to construct sequencing library. RNA-seq transcriptome library was prepared according to TruSeq™ RNA sample preparation Kit from Illumina (San Diego, CA). RNA-seq sequencing library was sequenced with Illumina Novaseq (2×150 bp read length). The processing of original images to sequences, base-calling, and quality value calculations were performed using Illumina GA Pipeline (version 1.6).

Measuring formaldehyde concentration

To detect formaldehyde concentration in vivo, 1 mL culture solution was centrifuged, 12000 rpm, 4 °C, 5 min. The precipitate was collected and washed twice with PBS. Then, *E. coli* cells were broken by ultrasound after being re-suspended with 0.5 mL PBS, and the supernatant was obtained by centrifugation. The following conditions were used for detection by gas chromatography (GC): DB-WAX column, FID detector, column temperature of 80 °C, injector temperature of 200 °C, detector temperature of 350 °C.

DNA content analysis

Quantification of DNA content was conducted by taking 1 μ L samples and read by Qubit Flex fluorimeter. *E. coli* cells were incubated at 37 °C until OD_{600} reached 0.05. DNA replication inhibitor rifampicin was added to experimental groups and incubated for 90 min. *E. coli* cells were washed twice with PBS and then fixed with 100% cold MeOH for 1 h. The fixed cells were washed with PBS, and then DNA was stained with DAPI (4',6'-diamidino-2-phenylindole, 0.3 μ g mL⁻¹). For each time point, flow cytometry was used to analyze 20,000 cells. DAPI was excited with a UV laser at 355 nm and read at 450 nm. The number of the peaks of histograms showing amount of DNA in these cells corresponds to the number of fully replicated chromosomes and reflects the number of origins present in aggravated TRCs. In addition, 25 μ M cephalixin was added at time 0 to block cell division, followed by the addition of rifampicin after 40 min of incubation with cephalixin. The computer analysis software connected to flow cytometer analyzes the fluorescence intensity. There is a direct proportion between DNA content and fluorescence intensity. Number of genome equivalents (N) was calculated using stationary phase cells (1N) as a reference. The doubling of DNA replication is determined by calculating the multiple relationship of the average fluorescence intensity.

Detection of the RNA: DNA hybrids by immunoblotting with S9.6 antibody

E. coli cells were incubated in LB medium at 37 °C until OD_{600} to 0.05. Total nucleic acids were extracted using a Genomic DNA kit (TIANGEN). 1 μ g of DNA from each sample was labeled on Hybond-N+ nylon membrane (Sangon biotech) with a vacuum slot blotting. Then, the membrane was crosslinked with UV light (0.12 J/m²), sealed with 5% milk /TBST (Tris buffered brine + 0.5% Tween 20-Bio-RAD) and incubated at 4 °C overnight. 1 μ g of anti-RNA: DNA hybrid antibodies (S9.6 mouse antibody, Kerfast, ENH001) was added to 1% milk /TBST and incubated at 4 °C for 2 h. After washing with TBST for 3 times, the secondary antibody (1:10,000 goat anti-mouse HRP, catalog no. A0216; Beyotime) was added at room temperature for 1 h. The membrane was washed 3 times with TBST and detected with a SuperFemto ECL Chemiluminescence Kit (Vazyme). Fluorescence images were taken using the Invitrogen iBright gel imaging system (Thermo Fisher), and the blots were quantitatively analyzed using the ImageJ software.

qRT-PCR assay

The methylotrophic *E. coli* cells were cultivated and then washed by DEPC-treated water. The MiniBEST universal RNA extraction kit (Takara Bio, Dalian, China) was used to extract total RNA, and cDNA was synthesized by the PrimeScript II first-strand cDNA synthesis kit (Takara Bio, Dalian, China). After that, the quantitative mRNA levels were determined with *16S rRNA* as a reference gene using TB Green qPCR Master Mix (Takara Bio, Dalian, China) in Bio-Rad CFX96 Touch (Bio-Rad, the United States).

Measuring expression of fluorescent protein-based protein interactions

Overnight cultures expressing TOPAI, EcTopoI, and co-expressing TOPAI and EcTopoI were diluted by 1/100, prepared with 2 μ L and photographed using a focal fluorescence microscope (Leica TCS SP8) using a $\times 60$ oil objective lens. For the mVenus based reporter protein, the analysis was performed using excitation at 490 nm and emission at 530 nm.

Fluorescence intensity analysis

Fluorescence microscopy was performed with a confocal microscope (Leica TCS SP8) using a $\times 60$ oil objective lens. The number of *E. coli* cells and fluorescence intensity were measured and counted in images using ImageJ software. *E. coli* cells for data analysis were randomly selected ($n = 20 - 30$ cells, three independent experiments). ImageJ (NIH, <http://rsbweb.nih.gov/ij/>) was used for measuring the fluorescence intensity of *E. coli* cells. Microsoft Excel 2019 and Origin 2023 (www.originlab.com) were used for graphing and statistical analysis.

Assay methods

OD_{600} was measured using a spectrophotometer. Methanol was measured according to the procedure described previously²⁶. In brief, the culture was centrifuged and filtered to prepare the sample. Methanol concentration was determined by an Agilent Technologies 7890 gas chromatography with a flame-ionization-detector. The concentration of glycolaldehyde was determined by high-performance liquid chromatography using an Aminex HPX-87H column (7.8 \times 300 mm; Bio-Rad Laboratories, Inc., Hercules, CA, USA) at 45 °C with 0.05 mmol/L phase sulfuric acid as the mobile phase. For fructose-6-phosphate quantification, the reaction mixture was centrifuged at 18514 $\times g$ for 10 min, and the supernatant was collected. For the Acetyl-CoA assay, *E. coli* cells were washed with a PBS buffer (pH 7.4). The cell pellet was normalized to an optical density of 1 and used for Acetyl-CoA analysis with ELISA Kit (Sangon Biotech, No. D751001)⁶⁹.

Statistical and reproducibility

The significance of data was determined by a two-tailed Student's *t*-test by SPSS statistics software (SPSS R24.0.0). Significant differences were marked as * $P < 0.05$, ** $P < 0.01$ and *** $P < 0.001$. All data were presented as mean \pm s.e.m. All experiments in this study were performed in three biological repeats.

Reporting summary

Further information on research design is available in the Nature Portfolio Reporting Summary linked to this article.

Data availability

Genome and transcriptome resequencing raw files are available at Genome Sequence Archive with BioProject ID CRA015159 [<https://ngdc.cncb.ac.cn/gsa/s/i9N1r5D9>]. Source data are provided with this paper, which is also available at Figshare [<https://figshare.com/s/591bbe9bc76526d123a1>]. Source data are provided with this paper.

References

- Jouny, M., Luc, W. & Jiao, F. General techno-economic analysis of CO₂ electrolysis systems. *Ind. Eng. Chem. Res* **57**, 2165–2177 (2018).
- Musa, S. D., Zhonghua, T., Ibrahim, A. O. & Habib, M. China's energy status: a critical look at fossils and renewable options. *Renew. Sust. Energ. Rev.* **81**, 2281–2290 (2018).
- Singh, A. K., Kishore, G. M. & Pakrasi, H. B. Emerging platforms for co-utilization of one-carbon substrates by photosynthetic organisms. *Curr. Opin. Biotechnol.* **53**, 201–208 (2018).
- Herrera-Estrella, A., Šmejkalová, H., Erb, T. J. & Fuchs, G. Methanol assimilation in *Methylobacterium extorquens* AM1: demonstration of all enzymes and their regulation. *PLoS One* **5**, e13001 (2010).
- Jiang, W. et al. Metabolic engineering strategies to enable microbial utilization of C1 feedstocks. *Nat. Chem. Biol.* **17**, 845–855 (2021).
- Claassens, N. J., Sousa, D. Z., Dos Santos, V. A., de Vos, W. M. & van der Oost, J. Harnessing the power of microbial autotrophy. *Nat. Rev. Microbiol.* **14**, 692–706 (2016).
- Hu, G. P. et al. Light-driven CO₂ sequestration in *Escherichia coli* to achieve theoretical yield of chemicals. *Nat. Catal.* **4**, 395–406 (2021).
- Muller, J. E. N. et al. Engineering *Escherichia coli* for methanol conversion. *Metab. Eng.* **28**, 190–201 (2015).
- Whitaker, W. B. et al. Engineering the biological conversion of methanol to specialty chemicals in *Escherichia coli*. *Metab. Eng.* **39**, 49–59 (2017).
- Bennett, R. K., Gonzalez, J. E., Whitaker, W. B., Antoniewicz, M. R. & Papoutsakis, E. T. Expression of heterologous non-oxidative pentose phosphate pathway from *Bacillus methanolicus* and phosphoglucose isomerase deletion improves methanol assimilation and metabolite production by a synthetic *Escherichia coli* methylotroph. *Metab. Eng.* **45**, 75–85 (2018).
- Chen, C. T. et al. Synthetic methanol auxotrophy of *Escherichia coli* for methanol-dependent growth and production. *Metab. Eng.* **49**, 257–266 (2018).
- Gonzalez, J. E., Bennett, R. K., Papoutsakis, E. T. & Antoniewicz, M. R. Methanol assimilation in *Escherichia coli* is improved by co-utilization of threonine and deletion of leucine-responsive regulatory protein. *Metab. Eng.* **45**, 67–74 (2018).
- Meyer, F. et al. Methanol-essential growth of *Escherichia coli*. *Nat. Commun.* **9**, 1508 (2018).
- Woolston, B. M., King, J. R., Reiter, M., Van Hove, B. & Stephanopoulos, G. Improving formaldehyde consumption drives methanol assimilation in engineered *E. coli*. *Nat. Commun.* **9**, 2387 (2018).
- Yu, H. & Liao, J. C. A modified serine cycle in *Escherichia coli* converts methanol and CO₂ to two-carbon compounds. *Nat. Commun.* **9**, 3992 (2018).
- Bennett, R. K. et al. Triggering the stringent response enhances synthetic methanol utilization in *Escherichia coli*. *Metab. Eng.* **61**, 1–10 (2020).
- Bennett, R. K. et al. Engineering *Escherichia coli* for methanol-dependent growth on glucose for metabolite production. *Metab. Eng.* **60**, 45–55 (2020).
- De Simone, A. et al. Mixing and matching methylotrophic enzymes to design a novel methanol utilization pathway in *E. coli*. *Metab. Eng.* **61**, 315–325 (2020).
- Espinosa, M. I. et al. Adaptive laboratory evolution of native methanol assimilation in *Saccharomyces cerevisiae*. *Nat. Commun.* **11**, 5564 (2020).
- He, H., Hoper, R., Dodenhof, M., Marliere, P. & Bar-Even, A. An optimized methanol assimilation pathway relying on promiscuous formaldehyde-condensing aldolases in *E. coli*. *Metab. Eng.* **60**, 1–13 (2020).
- Keller, P. et al. Methanol-dependent *Escherichia coli* strains with a complete ribulose monophosphate cycle. *Nat. Commun.* **11**, 5403 (2020).
- Cai, P. et al. Methanol biotransformation toward high-level production of fatty acid derivatives by engineering the industrial yeast *Pichia pastoris*. *Proc. Natl Acad. Sci.* **119**, e2201711119 (2022).
- Keller, P. et al. Generation of an *Escherichia coli* strain growing on methanol via the ribulose monophosphate cycle. *Nat. Commun.* **13**, 5243 (2022).
- Zhan, C. et al. Reprogramming methanol utilization pathways to convert *Saccharomyces cerevisiae* to a synthetic methylotroph. *Nat. Catal.* **6**, 435–450 (2023).
- Kim, S. et al. Growth of *E. coli* on formate and methanol via the reductive glycine pathway. *Nat. Chem. Biol.* **16**, 538–545 (2020).
- Chen, F. Y., Jung, H. W., Tsuei, C. Y. & Liao, J. C. Converting *Escherichia coli* to a synthetic methylotroph growing solely on methanol. *Cell* **182**, 933–946 (2020).
- Gao, J., Li, Y., Yu, W. & Zhou, Y. J. Rescuing yeast from cell death enables overproduction of fatty acids from sole methanol. *Nat. Metab.* **4**, 932–943 (2022).
- Witthoff, S. et al. Metabolic engineering of *Corynebacterium glutamicum* for methanol metabolism. *Appl Environ. Microbiol.* **81**, 2215–2225 (2015).
- Wang X., et al. Biological conversion of methanol by evolved *Escherichia coli* carrying a linear methanol assimilation pathway. *Bioresour. Bioprocess.* **4**, 41 (2017).
- He, H., Edlich-Muth, C., Lindner, S. N. & Bar-Even, A. Ribulose monophosphate shunt provides nearly all biomass and energy required for growth of *E. coli*. *ACS Synth. Biol.* **7**, 1601–1611 (2018).
- Bogorad, I. W. et al. Building carbon-carbon bonds using a biocatalytic methanol condensation cycle. *Proc. Natl Acad. Sci.* **111**, 15928–15933 (2014).
- Siegel, J. B. et al. Computational protein design enables a novel one-carbon assimilation pathway. *Proc. Natl Acad. Sci.* **112**, 3704–3709 (2015).
- Chou, A., Clomburg, J. M., Qian, S. & Gonzalez, R. 2-Hydroxyacyl-CoA lyase catalyzes acyloin condensation for one-carbon bioconversion. *Nat. Chem. Biol.* **15**, 900–906 (2019).
- Lu, X. et al. Constructing a synthetic pathway for acetyl-coenzyme A from one-carbon through enzyme design. *Nat. Commun.* **10**, 1378 (2019).
- Yang, X. et al. Systematic design and in vitro validation of novel one-carbon assimilation pathways. *Metab. Eng.* **56**, 142–153 (2019).
- Wu, T. Y. et al. Characterization and evolution of an activator-independent methanol dehydrogenase from *Cupriavidus necator* N-1. *Appl Microbiol Biotechnol.* **100**, 4969–4983 (2016).
- Noor, E. et al. Pathway thermodynamics highlights kinetic obstacles in central metabolism. *PLoS Comput Biol.* **10**, 12 (2014).
- Noor, E. et al. The protein cost of metabolic fluxes: prediction from enzymatic rate laws and cost minimization. *PLoS Comput Biol.* **12**, e1005167 (2016).
- Bar-Even, A., Noor, E., Lewis, N. E. & Milo, R. Design and analysis of synthetic carbon fixation pathways. *Proc. Natl Acad. Sci. USA* **107**, 8889–8894 (2010).
- Wu, T. et al. Engineering a synthetic energy-efficient formaldehyde assimilation cycle in *Escherichia coli*. *Nat. Commun.* **14**, 8490 (2023).
- Cotton, C. A. R., Claassens, N. J., Benito-Vaquero, S. & Bar-Even, A. Renewable methanol and formate as microbial feedstocks. *Curr. Opin. Biotechnol.* **62**, 168–180 (2020).
- Söhling, B. & Gottschalk, G. Molecular analysis of the anaerobic succinate degradation pathway in *Clostridium kluyveri*. *J. bacteriol.* **178**, 871–880 (1996).
- Eom, G. E., Lee, H. & Kim, S. Development of a genome-targeting mutator for the adaptive evolution of microbial cells. *Nucleic Acids Res* **50**, e38 (2022).
- Tehranchi, A. K. et al. The transcription factor DksA prevents conflicts between DNA replication and transcription machinery. *Cell* **141**, 595–605 (2010).

45. Gyenis, A. et al. Genome-wide RNA polymerase stalling shapes the transcriptome during aging. *Nat. Genet* **55**, 268–279 (2023).
46. Campbell, E. A. et al. Structural mechanism for rifampicin inhibition of bacterial RNA polymerase. *Cell* **104**, 901–912 (2001).
47. Conrad, T. M. et al. RNA polymerase mutants found through adaptive evolution reprogram *Escherichia coli* for optimal growth in minimal media. *Proc. Natl Acad. Sci.* **107**, 20500–20505 (2010).
48. Gines-Candelaria, E., Blinkova, A. & Walker, J. R. Mutations in *Escherichia coli* *dnaA* which suppress a *dnaX* (Ts) polymerization mutation and are dominant when located in the chromosomal allele and recessive on plasmids. *J. bacteriol.* **177**, 705–715 (1995).
49. Wiedermannova, J. & Krasny, L. β -CASP proteins removing RNA polymerase from DNA: when a torpedo is needed to shoot a sitting duck. *Nucleic Acids Res* **49**, 10221–10234 (2021).
50. Hawkins, M. et al. Direct removal of RNA polymerase barriers to replication by accessory replicative helicases. *Nucleic Acids Res* **47**, 5100–5113 (2019).
51. Akbalik, G. et al. Visualization of newly synthesized neuronal RNA in vitro and in vivo using click-chemistry. *RNA Biol.* **14**, 20–28 (2016).
52. Sutormin, D. et al. Interaction between transcribing RNA polymerase and topoisomerase I prevents R-loop formation in *E. coli*. *Nat. Commun.* **13**, 4524 (2022).
53. Bou-Nader, C., Bothra, A., Garboczi, D. N., Leppla, S. H. & Zhang, J. Structural basis of R-loop recognition by the S9.6 monoclonal antibody. *Nat. Commun.* **13**, 1641 (2022).
54. Fleurier, S., Dapa, T., Tenaillon, O., Condon, C. & Matic, I. rRNA operon multiplicity as a bacterial genome stability insurance policy. *Nucleic Acids Res* **50**, 12601–12620 (2022).
55. He, H. et al. In vivo rate of formaldehyde condensation with tetrahydrofolate. *Metabolites* **10**, 65 (2020).
56. Yamaguchi, Y. & Inouye, M. An endogenous protein inhibitor, YjhX (TopAI), for topoisomerase I from *Escherichia coli*. *Nucleic Acids Res* **43**, 10387–10396 (2015).
57. Liu, H. et al. Enhancing biofuels production by engineering the actin cytoskeleton in *Saccharomyces cerevisiae*. *Nat. Commun.* **13**, 1886 (2022).
58. Ochsner, A. M., Sonntag, F., Buchhaupt, M., Schrader, J. & Vorholt, J. A. *Methylobacterium extorquens*: methylotrophy and biotechnological applications. *Appl Microbiol Biotechnol.* **99**, 517–534 (2014).
59. Kato, N., Yurimoto, H. & Thauer, R. K. The physiological role of the ribulose monophosphate pathway in bacteria and archaea. *Biosci. biotechnol. biochem* **70**, 10–21 (2006).
60. Zhang, W. et al. Guidance for engineering of synthetic methylotrophy based on methanol metabolism in methylotrophy. *RSC Adv.* **7**, 4083–4091 (2017).
61. Dedysh, S. N. et al. Methylotrophic Autotrophy in *Beijerinckia mobilis*. *J. Bacteriol.* **187**, 3884–3888 (2005).
62. Gleizer, S. et al. Conversion of *Escherichia coli* to generate all biomass carbon from CO₂. *Cell* **179**, 1255–1263 (2019).
63. Koopman, F. W., de Winde, J. H. & Ruijsenaars, H. J. C1 compounds as auxiliary substrate for engineered *Pseudomonas putida* S12. *Appl Microbiol Biotechnol.* **83**, 705–713 (2009).
64. Reiter, M. A. et al. A synthetic methylotrophic *Escherichia coli* as a chassis for bioproduction from methanol. *Nat. Catal.* **7**, 560–573 (2024).
65. Nieh, L.-Y. et al. Evolutionary engineering of methylotrophic *E. coli* enables fast growth on methanol. *Nat. Commun.* **15**, 8840 (2024).
66. Kao, K. C., Nayak, D. D. & Marx, C. J. Genetic and phenotypic comparison of facultative methylotrophy between *Methylobacterium extorquens* strains PA1 and AM1. *PLoS One* **9**, e107887 (2014).
67. Wang, Y. et al. Adaptive laboratory evolution enhances methanol tolerance and conversion in engineered *Corynebacterium glutamicum*. *Commun. Biol.* **3**, 217 (2020).
68. Fujioka, Y. et al. Phase separation organizes the site of autophagosome formation. *Nature* **578**, 301–305 (2020).
69. Lee, Y., Cho, H. J., Choi, J. I. & Woo, H. M. Hybrid embden-meyerhof-parnas pathway for reducing CO₂ loss and increasing the acetyl-CoA levels during microbial fermentation. *ACS Sustain Chem. Eng.* **9**, 12394–12405 (2021).

Acknowledgements

This work is supported by the Key Program of the National Natural Science Foundation of China (22038005) to L.L., the Major Project of Natural Science Foundation of Jiangsu Province (BK20220022 to J.W. and BK20212013 to L.L.).

Author contributions

X.M. and L.L. conceived the project and wrote the manuscript. X.M., G.H., X.L., C.G., W.S., W.W. and J.W. designed and performed all the experiments. X.M. and L.L. analyzed the results.

Competing interests

The authors declare no competing interests.

Additional information

Supplementary information The online version contains supplementary material available at <https://doi.org/10.1038/s41467-024-55502-5>.

Correspondence and requests for materials should be addressed to Liming Liu.

Peer review information *Nature Communications* thanks Michelle Hawkins, who co-reviewed with Aisha SyedaNico Claassens, Kazuyuki Shimizu and the other, anonymous, reviewer(s) for their contribution to the peer review of this work. A peer review file is available.

Reprints and permissions information is available at <http://www.nature.com/reprints>

Publisher's note Springer Nature remains neutral with regard to jurisdictional claims in published maps and institutional affiliations.

Open Access This article is licensed under a Creative Commons Attribution-NonCommercial-NoDerivatives 4.0 International License, which permits any non-commercial use, sharing, distribution and reproduction in any medium or format, as long as you give appropriate credit to the original author(s) and the source, provide a link to the Creative Commons licence, and indicate if you modified the licensed material. You do not have permission under this licence to share adapted material derived from this article or parts of it. The images or other third party material in this article are included in the article's Creative Commons licence, unless indicated otherwise in a credit line to the material. If material is not included in the article's Creative Commons licence and your intended use is not permitted by statutory regulation or exceeds the permitted use, you will need to obtain permission directly from the copyright holder. To view a copy of this licence, visit <http://creativecommons.org/licenses/by-nc-nd/4.0/>.

© The Author(s) 2024